AGU PUBLICATIONS

Journal of Geophysical Research: Solid Earth

Supporting Information for

Glacial-interglacial circulation and climatic changes in the South Indian Ocean (Kerguelen Plateau region) recorded by detrital and biogenic magnetic minerals

Yan Liu[1,2,3,4], Catherine Kissel[5], Alain Mazaud[5], Yongxin Pan[1,4], Jinhua Li[1,2,4]*

[1]Key Laboratory of Earth and Planetary Physics, Institute of Geology and Geophysics, Chinese Academy of Sciences, Beijing 100029, China, [2]Laboratory for Marine Geology, Qingdao National Laboratory for Marine Science and Technology, Qingdao 266071, China, [3]Southern Marine Science and Engineering Guangdong Laboratory, Zhuhai 519082, China, [4]University of Chinese Academy Sciences, Beijing 100029, China, [5]Laboratoire des Sciences du Climat et de l'Environnement/IPSL, CEA, CNRS, UVSQ, Université Paris-Saclay, 91190 Gif-sur-Yvette Cedex, France.

Contents of this file

Figures S1-S12. Low-temperature and room-temperature rock magnetic measurements of twelve representative samples from the core MD11-3353. To characterize the magnetic mineral assemblages in the MD11-3353 core sediments, twenty-three discrete samples were selected across the core for systematically rock magnetic experiments. Twelve of them are shown here.

Figures S13-S31. Electron microscopic characterization of magnetic minerals from ten representative samples from the core MD11-3353. To accurately identify the origins of magnetic minerals in the MD11-3353 core sediments, sixteen of the twenty-three discrete samples were further magnetically extracted and then analyzed in detail by both scanning electron microscopy (SEM) and transmission electron microscopy (TEM) approaches. Ten of them are shown here.

Figures S32-S35. IRM unmixing results for the twenty-three selected samples from the core MD11-3353. To obtain a more accurate isothermal remanent magnetization (IRM) decomposition analyses, we decomposed the IRM acquisition curves with three, four and five magnetic coercivity components. Gradient of IRM-Unmixing component acquisition plot for six representative samples with three strategies are shown in Figure 32. Temporal variations of three, four and five magnetic components unmixed from IRM acquisition curves for core MD11-3353 over the past 150 kyrs are shown in Figure S33-S35.

Table S1. Magnetic parameters of the twenty-three selected sediment samples from the core MD11-3353.

Table S2. The relative content and abundance of detrital and biogenic magnetic minerals for the twenty-three selected sediment samples from the core MD11-3353.

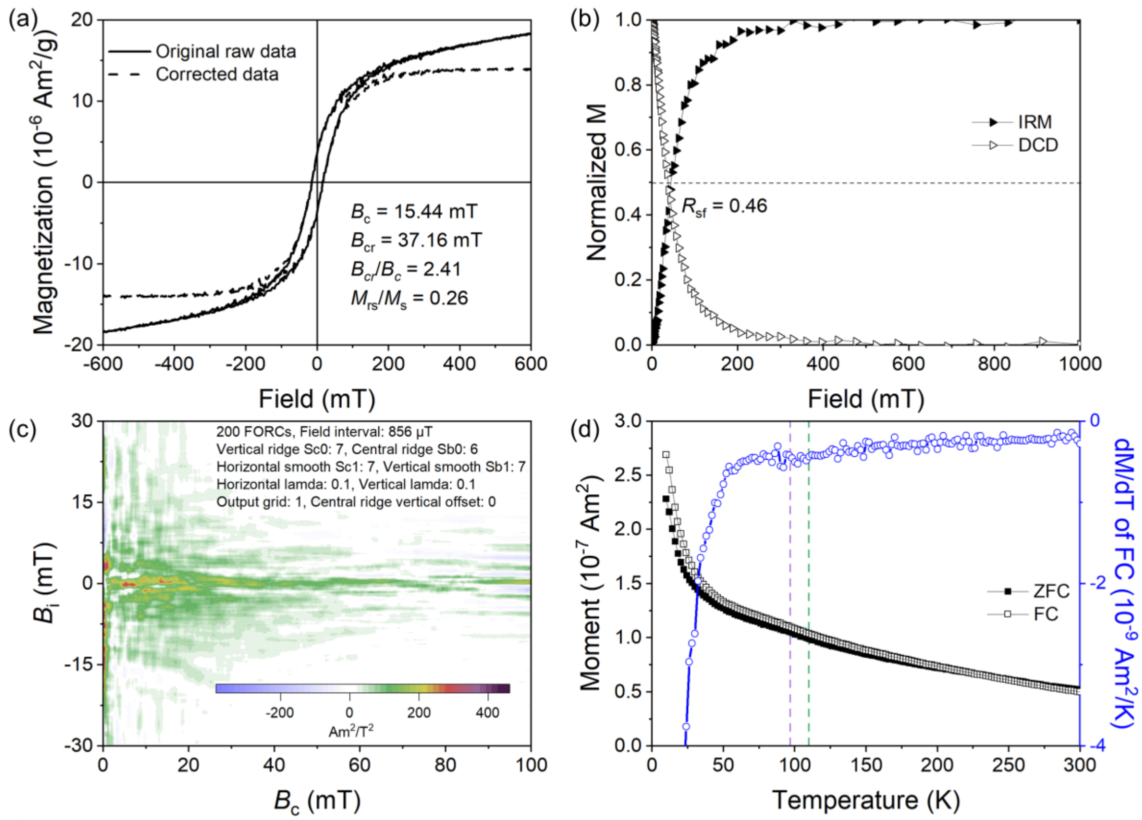

Figure S1. Rock magnetic properties for the sediment sample S1-1. (a) Room-temperature hysteresis loop (solid and dashed lines are the original raw and high-field slope-corrected data, respectively. (b) Normalized isothermal remanent magnetization (IRM) acquisition and direct current demagnetization (DCD) curves. (c) First order reversal curves (FORC) diagram. (d) Field-cooled (FC)-SIRM$_{10\ K_2.5\ T}$ and Zero-field-cooled (ZFC)-SIRM$_{10\ K_2.5\ T}$ warming curves. The blue line with white circles in panel (d) is the first-order derivative curves of FC. Purple and green blue lines indicate the temperature points of ~97 K and ~110 K, respectively.

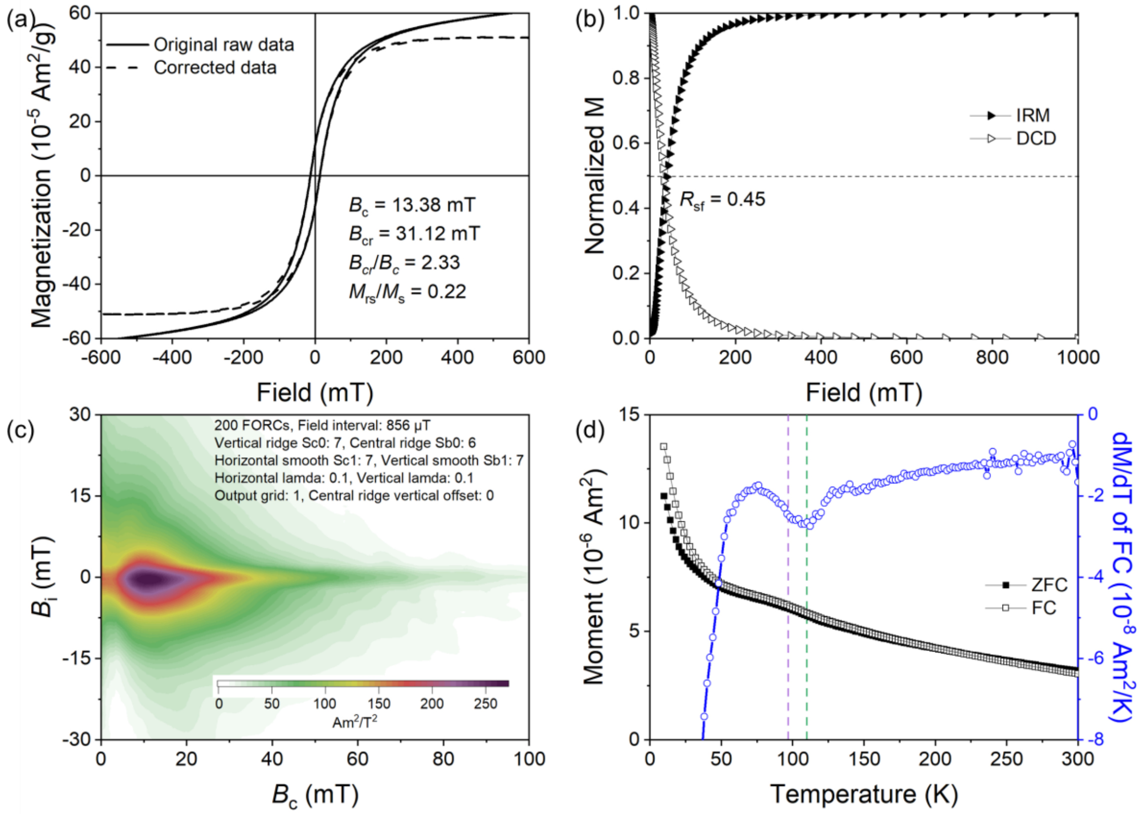

Figure S2. Rock magnetic properties for the sediment sample S2-2. (a) Room-temperature hysteresis loop (solid and dashed lines are the original raw and high-field slope-corrected data, respectively. (b) Normalized IRM acquisition and DCD curves. (c) FORC diagram. (d) FC-SIRM$_{10\ K_2.5\ T}$ and ZFC-SIRM$_{10\ K_2.5\ T}$ warming curves. The blue line with white circles in panel (d) is the first-order derivative curves of FC. Purple and green blue lines indicate the temperature points of ~97 K and ~110 K, respectively.

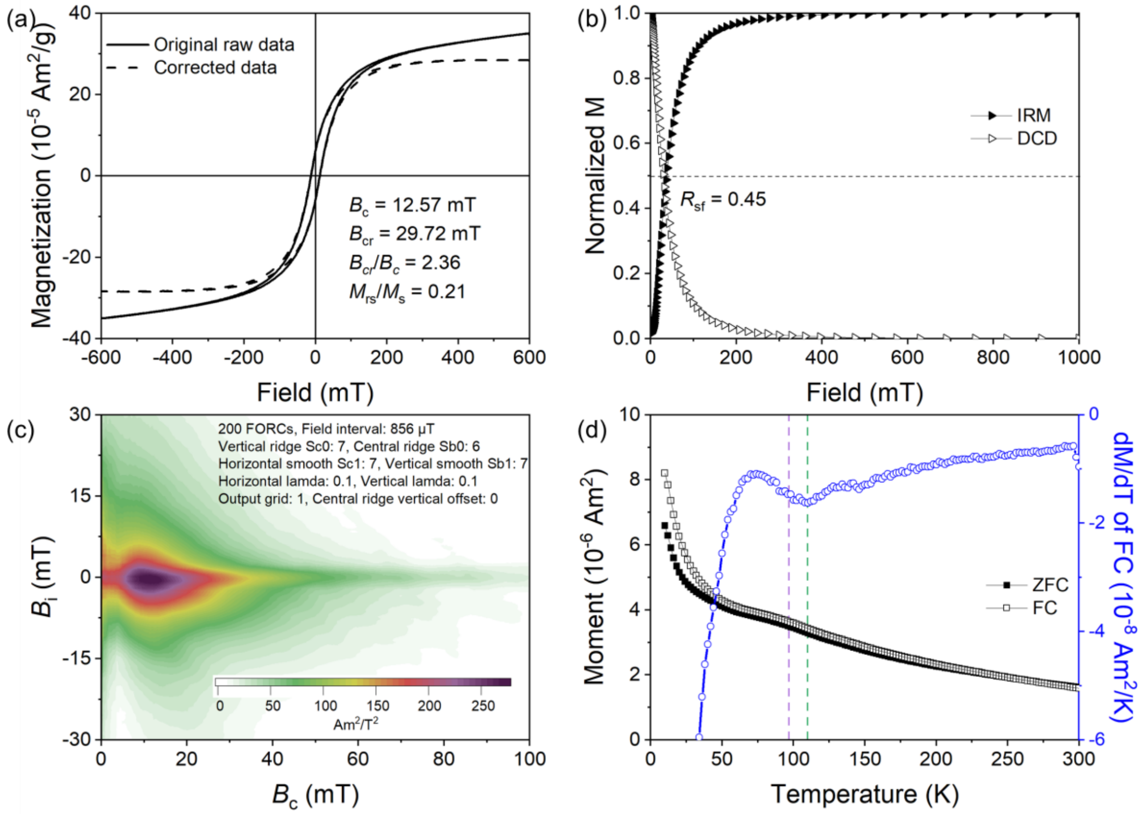

Figure S3. Rock magnetic properties for the sediment sample S3-2. (a) Room-temperature hysteresis loop (solid and dashed lines are the original raw and high-field slope-corrected data, respectively. (b) Normalized IRM acquisition and DCD curves. (c) FORC diagram. (d) FC-SIRM$_{10\ K_2.5\ T}$ and ZFC-SIRM$_{10\ K_2.5\ T}$ warming curves. The blue line with white circles in panel (d) is the first-order derivative curves of FC. Purple and green blue lines indicate the temperature points of ~97 K and ~110 K, respectively.

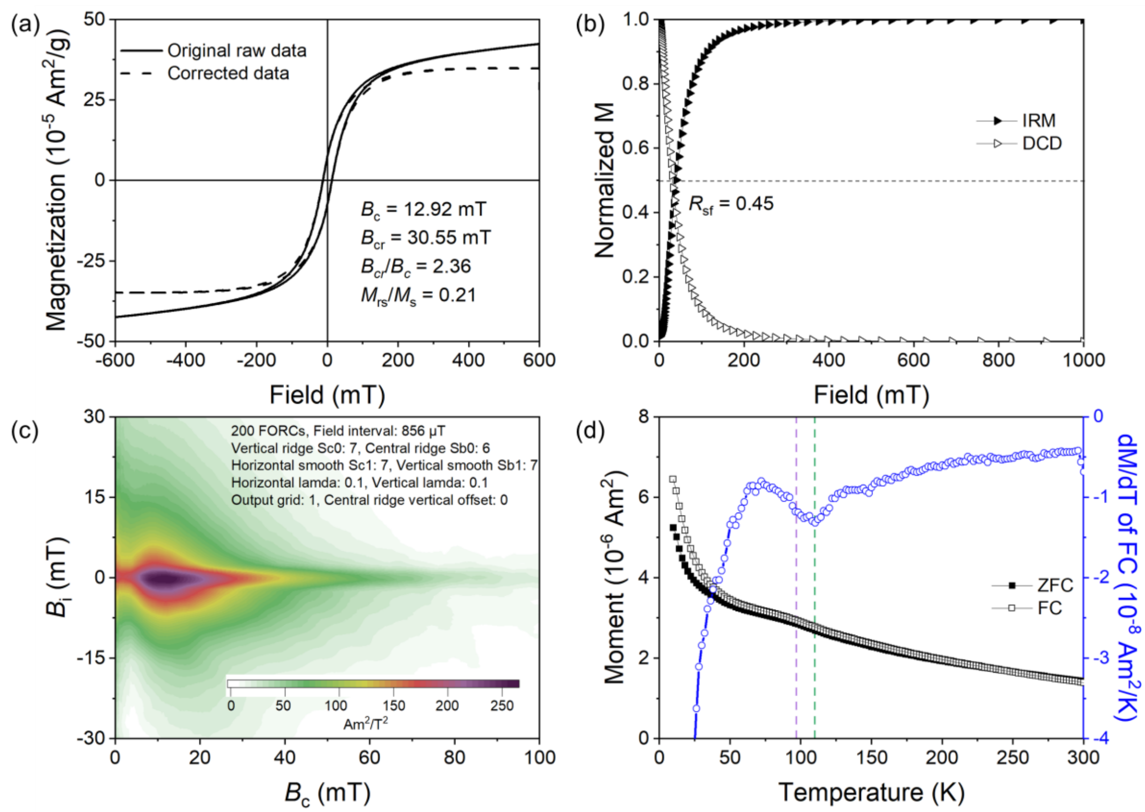

Figure S4. Rock magnetic properties for the sediment sample S4-1. (a) Room-temperature hysteresis loop (solid and dashed lines are the original raw and high-field slope-corrected data, respectively. (b) Normalized IRM acquisition and DCD curves. (c) FORC diagram. (d) FC-SIRM$_{10\ K_2.5\ T}$ and ZFC-SIRM$_{10\ K_2.5\ T}$ warming curves. The blue line with white circles in panel (d) is the first-order derivative curves of FC. Purple and green blue lines indicate the temperature points of ~97 K and ~110 K, respectively.

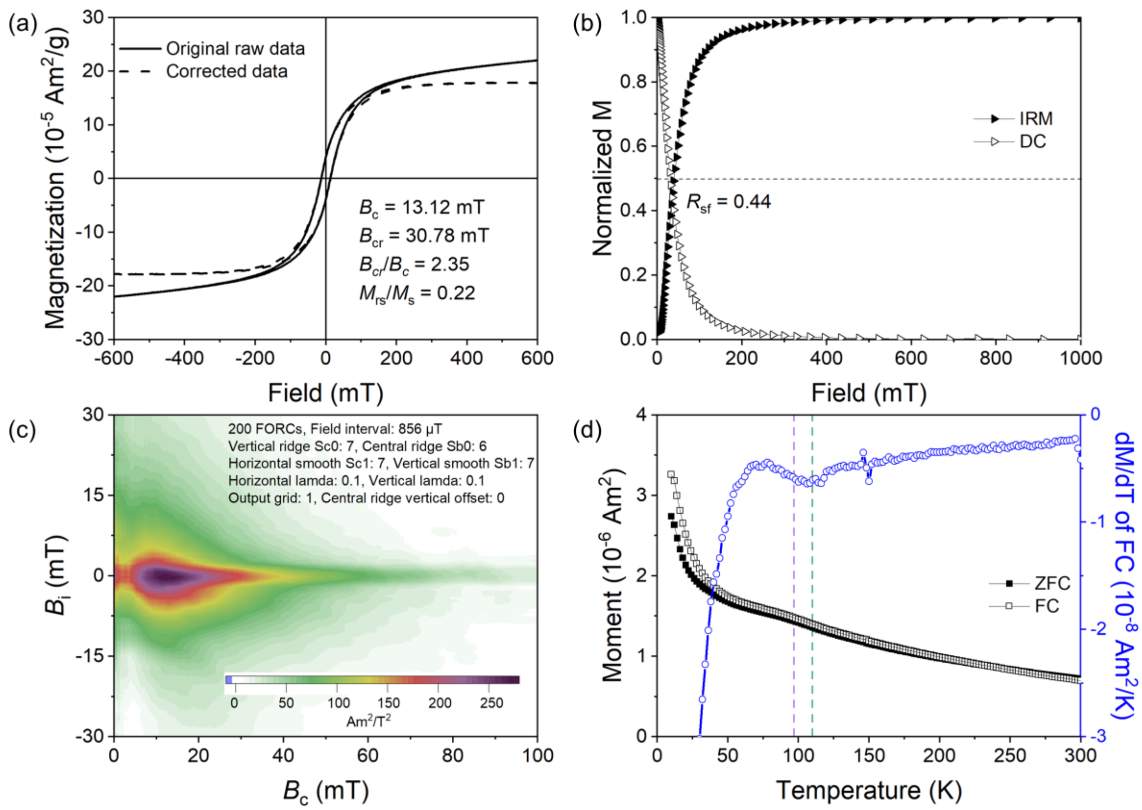

Figure S5. Rock magnetic properties for the sediment sample S4-2. (a) Room-temperature hysteresis loop (solid and dashed lines are the original raw and high-field slope-corrected data, respectively. (b) Normalized IRM acquisition and DCD curves. (c) FORC diagram. (d) FC-SIRM$_{10\ K_2.5\ T}$ and ZFC-SIRM$_{10\ K_2.5\ T}$ warming curves. The blue line with white circles in panel (d) is the first-order derivative curves of FC. Purple and green blue lines indicate the temperature points of ~97 K and ~110 K, respectively.

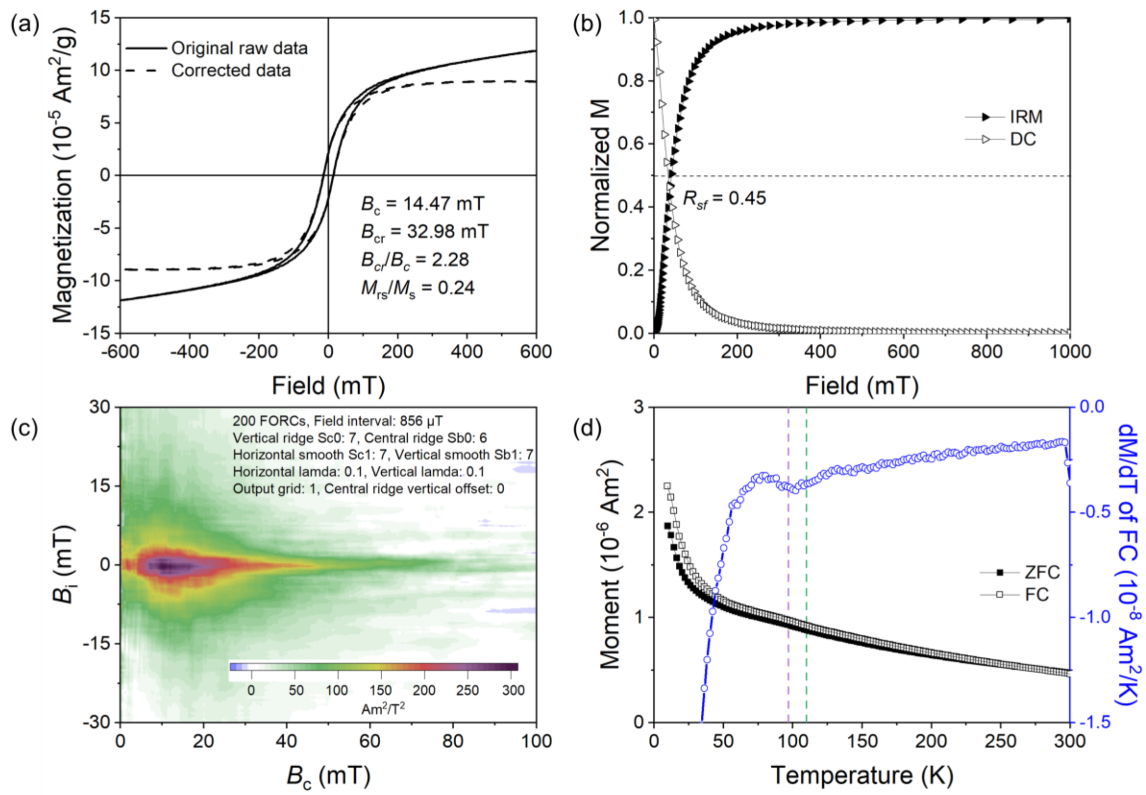

Figure S6. Rock magnetic properties for the sediment sample S4-3. (a) Room-temperature hysteresis loop (solid and dashed lines are the original raw and high-field slope-corrected data, respectively. (b) Normalized IRM acquisition and DCD curves. (c) FORC diagram. (d) FC-SIRM$_{10\ K_2.5\ T}$ and ZFC-SIRM$_{10\ K_2.5\ T}$ warming curves. The blue line with white circles in panel (d) is the first-order derivative curves of FC. Purple and green blue lines indicate the temperature points of ~97 K and ~110 K, respectively.

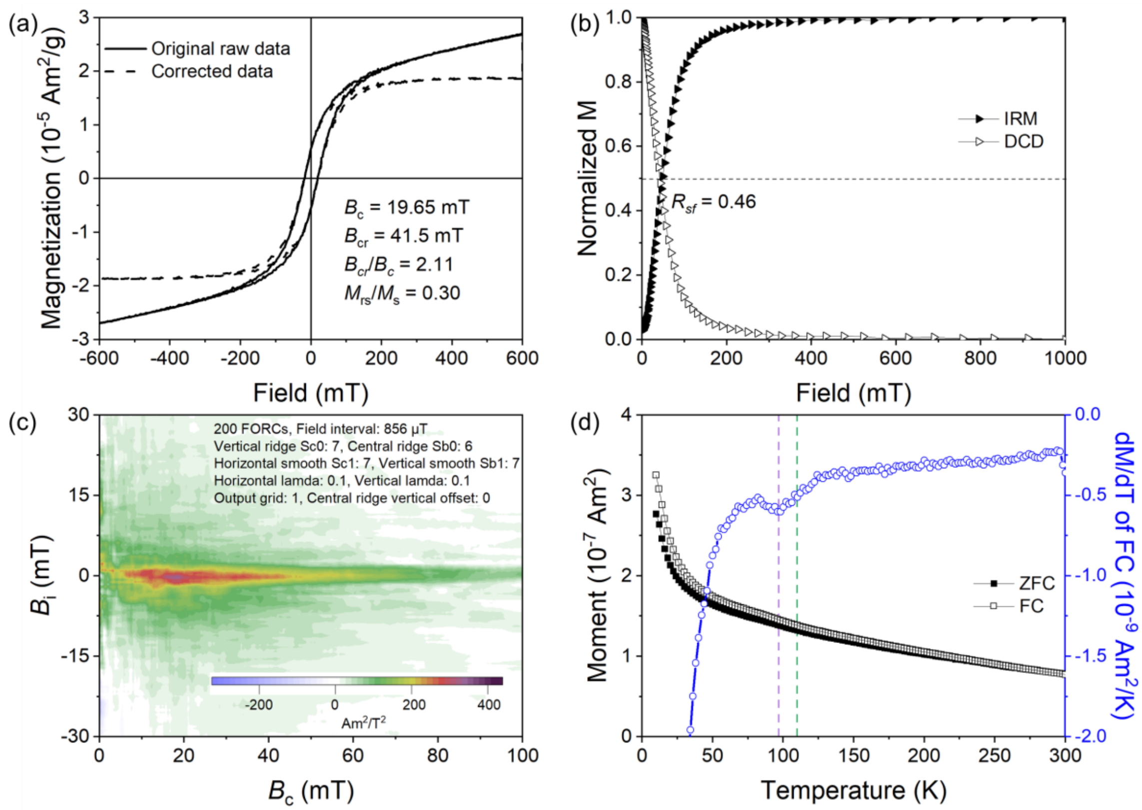

Figure S7. Rock magnetic properties for the sediment sample S5-1. (a) Room-temperature hysteresis loop (solid and dashed lines are the original raw and high-field slope-corrected data, respectively. (b) Normalized IRM acquisition and DCD curves. (c) FORC diagram. (d) FC-SIRM$_{10\ \mathrm{K_2.5\ T}}$ and ZFC-SIRM$_{10\ \mathrm{K_2.5\ T}}$ warming curves. The blue line with white circles in panel (d) is the first-order derivative curves of FC. Purple and green blue lines indicate the temperature points of ~97 K and ~110 K, respectively.

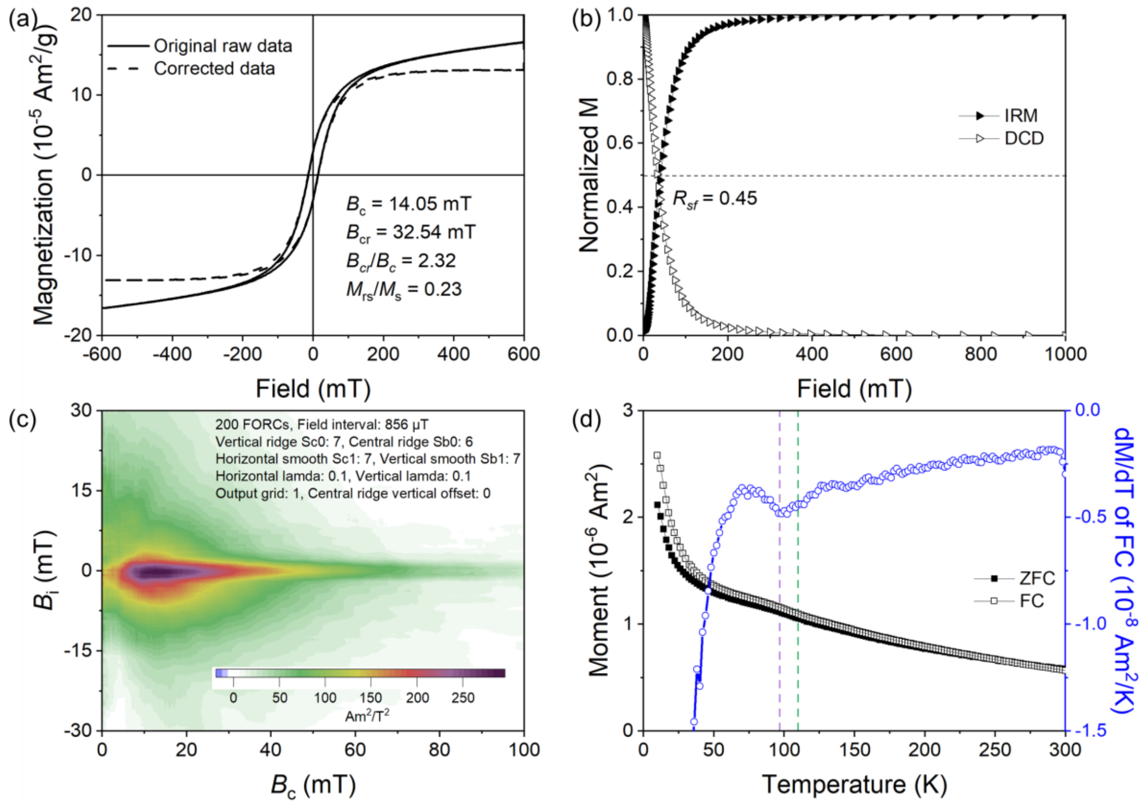

Figure S8. Rock magnetic properties for the sediment sample S5-3. (a) Room-temperature hysteresis loop (solid and dashed lines are the original raw and high-field slope-corrected data, respectively. (b) Normalized IRM acquisition and DCD curves. (c) FORC diagram. (d) FC-SIRM$_{10\ K_2.5\ T}$ and ZFC-SIRM$_{10\ K_2.5\ T}$ warming curves. The blue line with white circles in panel (d) is the first-order derivative curves of FC. Purple and green blue lines indicate the temperature points of ~97 K and ~110 K, respectively.

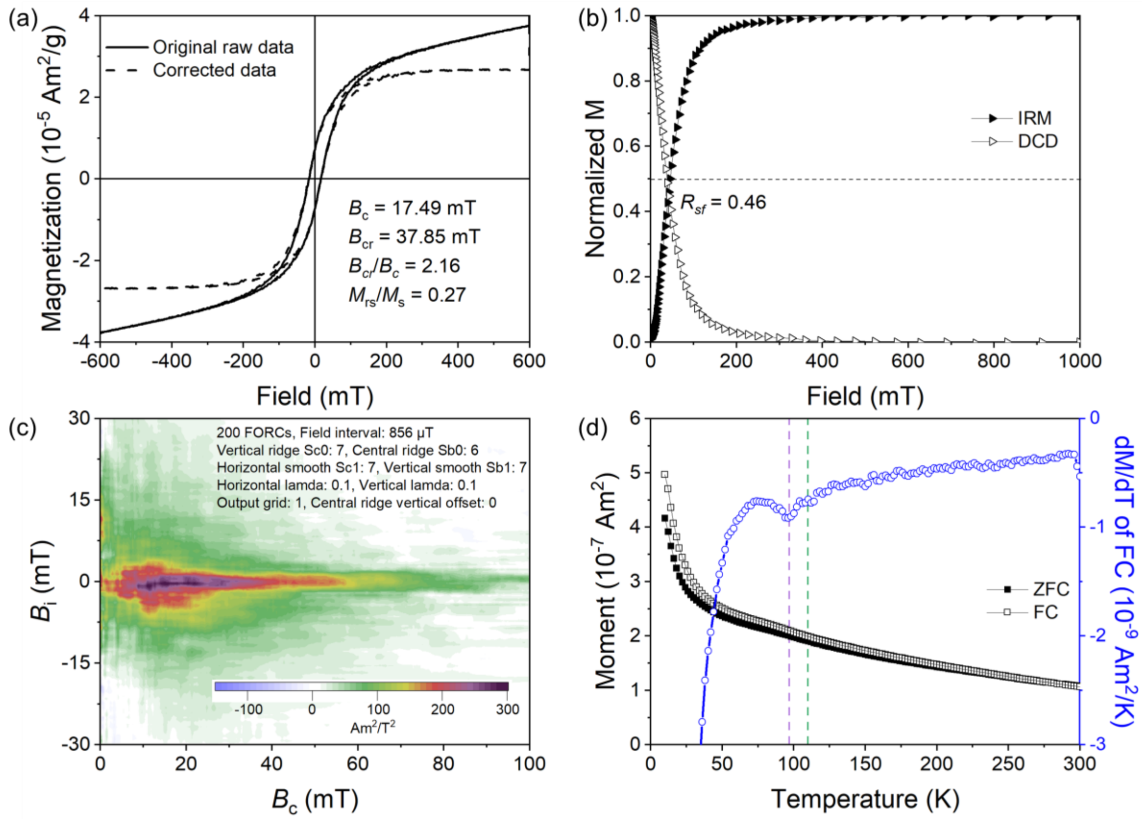

Figure S9. Rock magnetic properties for the sediment sample S5-5. (a) Room-temperature hysteresis loop (solid and dashed lines are the original raw and high-field slope-corrected data, respectively. (b) Normalized IRM acquisition and DCD curves. (c) FORC diagram. (d) FC-SIRM$_{10\ K_2.5\ T}$ and ZFC-SIRM$_{10\ K_2.5\ T}$ warming curves. The blue line with white circles in panel (d) is the first-order derivative curves of FC. Purple and green blue lines indicate the temperature points of ~97 K and ~110 K, respectively.

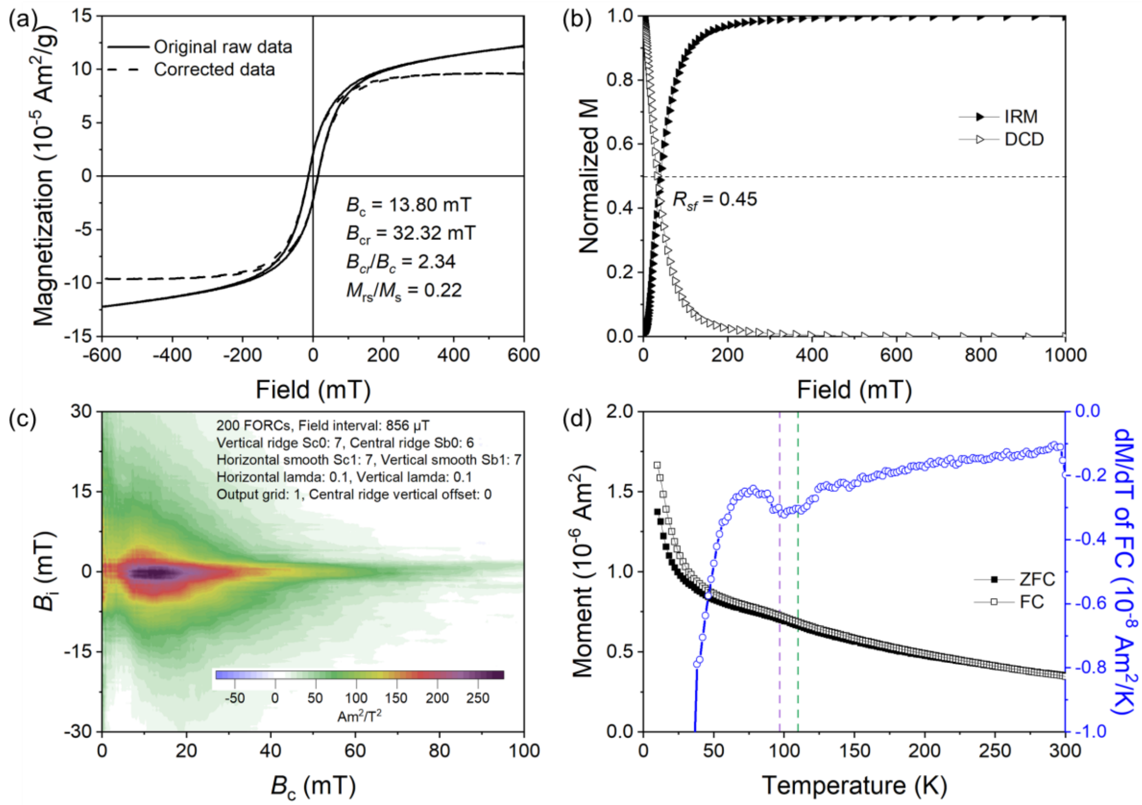

Figure S10. Rock magnetic properties for the sediment sample S5-9. (a) Room-temperature hysteresis loop (solid and dashed lines are the original raw and high-field slope-corrected data, respectively. (b) Normalized IRM acquisition and DCD curves. (c) FORC diagram. (d) FC-SIRM$_{10\ K_2.5\ T}$ and ZFC-SIRM$_{10\ K_2.5\ T}$ warming curves. The blue line with white circles in panel (d) is the first-order derivative curves of FC. Purple and green blue lines indicate the temperature points of ~97 K and ~110 K, respectively.

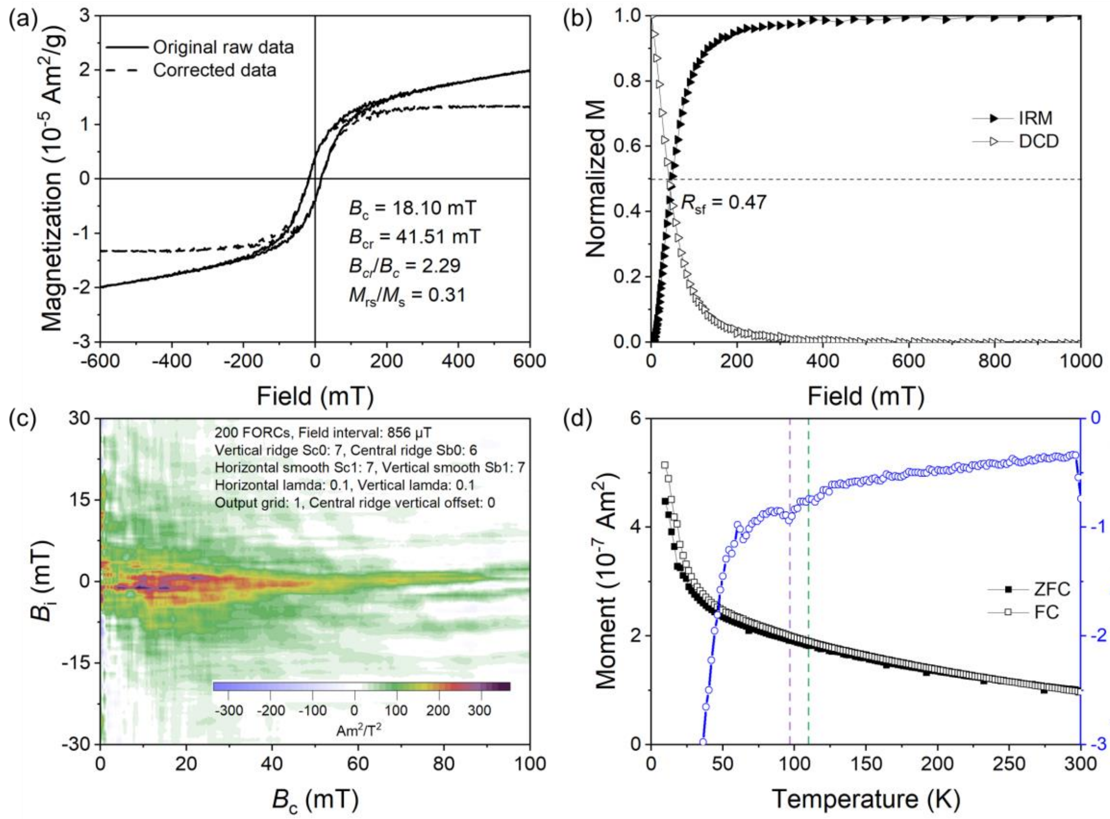

Figure S11. Rock magnetic properties for the sediment sample S5-11. (a) Room-temperature hysteresis loop (solid and dashed lines are the original raw and high-field slope-corrected data, respectively. (b) Normalized IRM acquisition and DCD curves. (c) FORC diagram. (d) FC-SIRM$_{10\ K_2.5\ T}$ and ZFC-SIRM$_{10\ K_2.5\ T}$ warming curves. The blue line with white circles in panel (d) is the first-order derivative curves of FC. Purple and green blue lines indicate the temperature points of ~97 K and ~110 K, respectively.

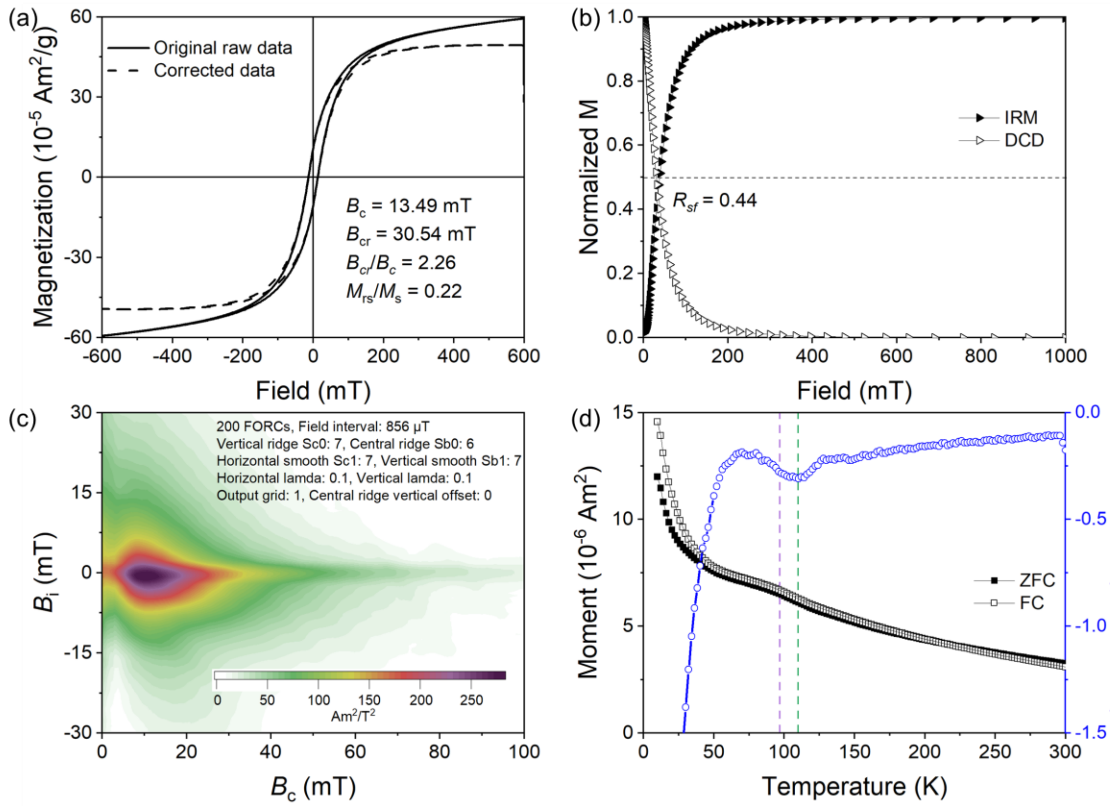

Figure S12. Rock magnetic properties for the sediment sample S6-2. (a) Room-temperature hysteresis loop (solid and dashed lines are the original raw and high-field slope-corrected data, respectively. (b) Normalized IRM acquisition and DCD curves. (c) FORC diagram. (d) FC-SIRM$_{10\ K_2.5\ T}$ and ZFC-SIRM$_{10\ K_2.5\ T}$ warming curves. The blue line with white circles in panel (d) is the first-order derivative curves of FC. Purple and green blue lines indicate the temperature points of ~97 K and ~110 K, respectively.

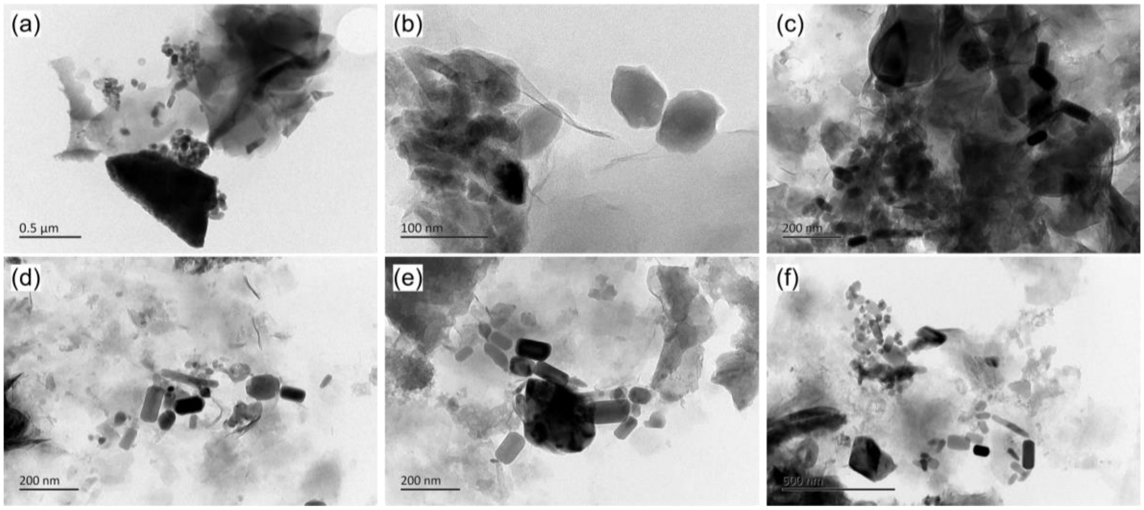

Figure S13. TEM images of magnetic minerals extracted from the sediment sample S1-1.

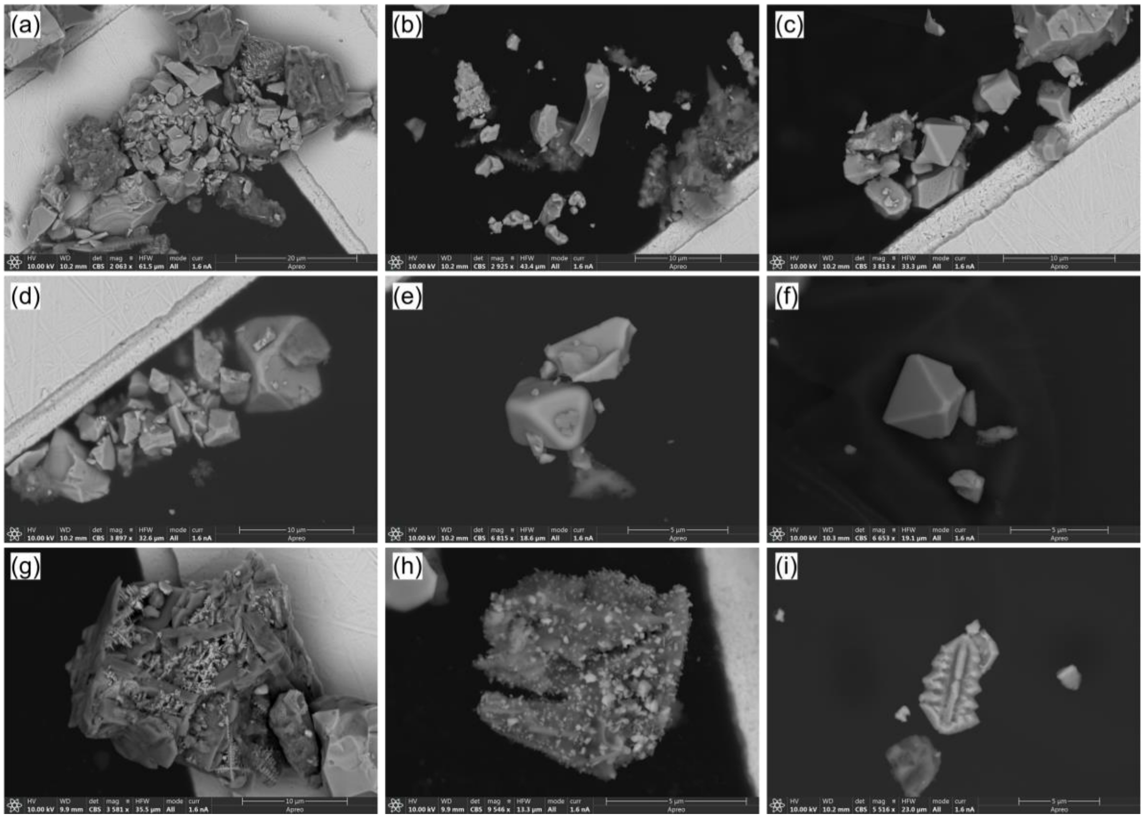

Figure S14. Backscattered SEM images of magnetic minerals extracted from the sediment sample S2-2.

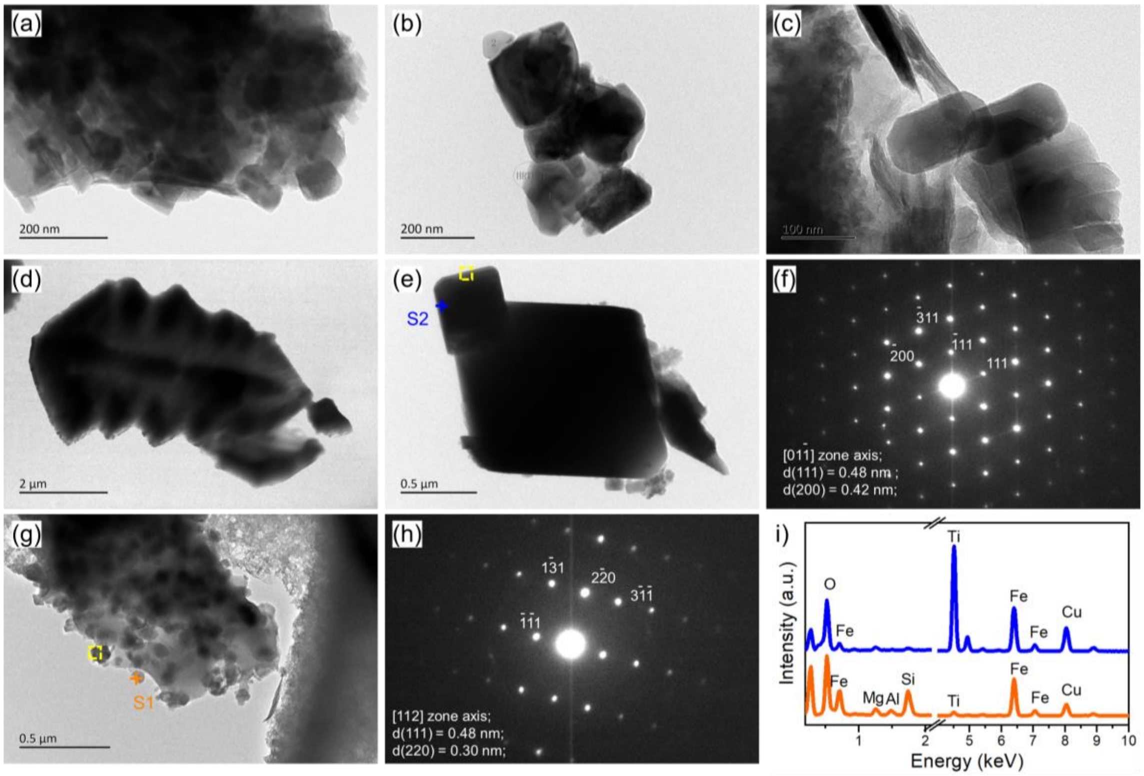

Figure S15. TEM images of magnetic minerals extracted from the sediment sample S2-2. (a)-(e), (g) TEM images. (f) SAED pattern recorded from [01$\bar{1}$] zone axis of the particle (indicated by yellow dashed box in (e)). (h) SAED pattern recorded from [112] zone axis of the particle (indicated by yellow dashed box in (g)). (i) TEM-based EDXS spectra for individual particles (indicated by colored crosses and names in (e) and (g).

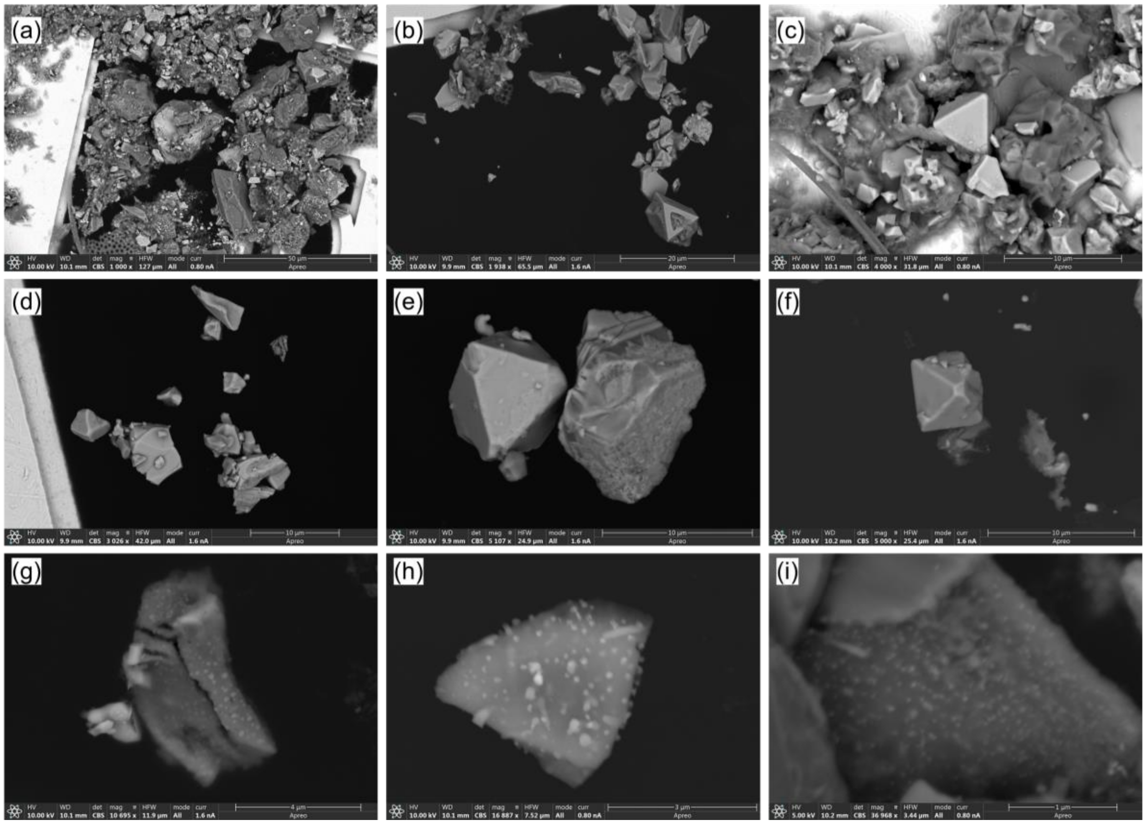

Figure S16. Backscattered SEM images of magnetic minerals extracted from the sediment sample S3-2.

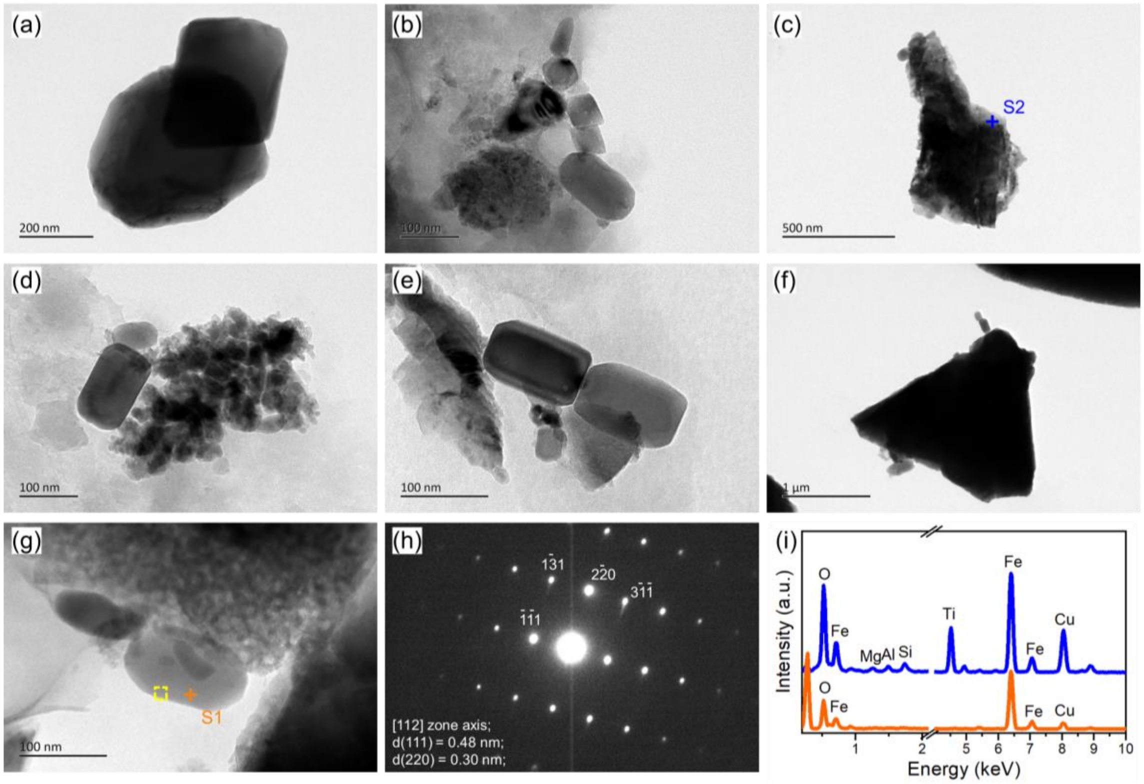

Figure S17. TEM images of magnetic minerals extracted from the sediment sample S3-2. (a)-(g) TEM images. (h) SAED pattern recorded from the [112] zone axis of the particle (indicated by yellow dashed box in (g)). (i) TEM-based EDXS spectra for individual particles (indicated by colored crosses and names in (c) and (g).

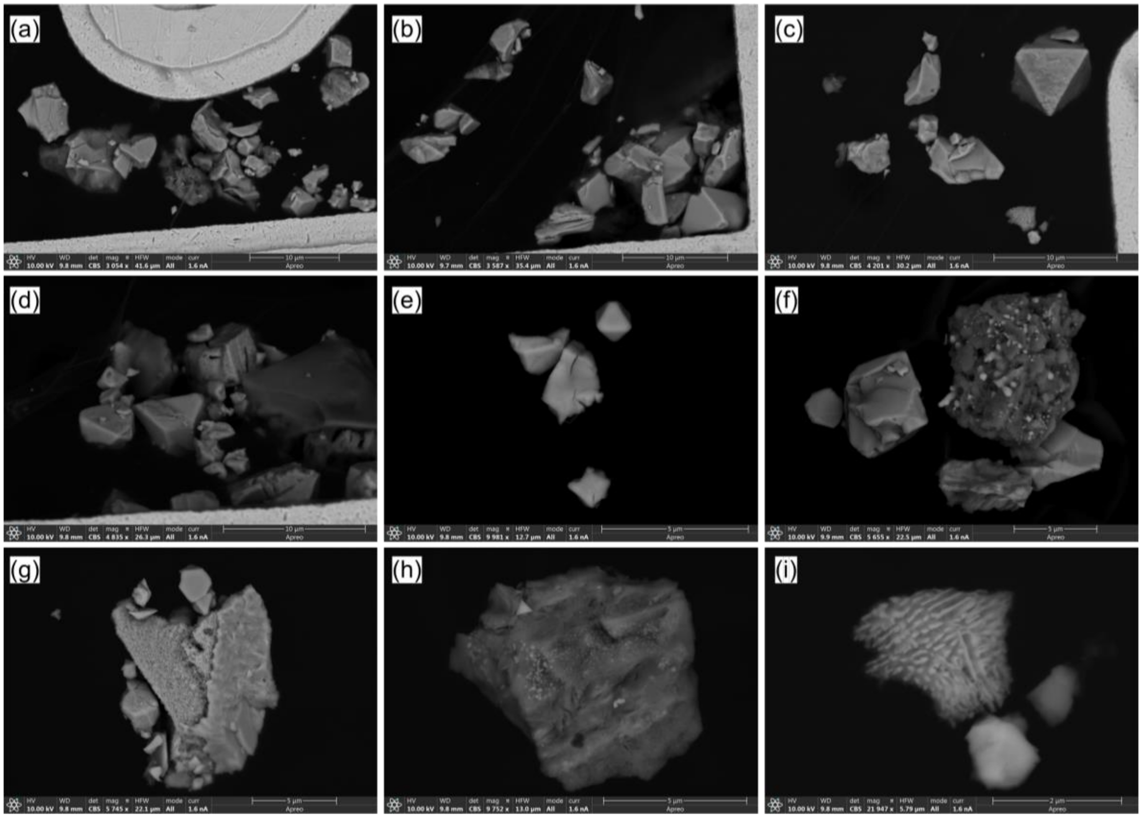

Figure S18. Backscattered SEM images of magnetic minerals extracted from the sediment sample S4-1.

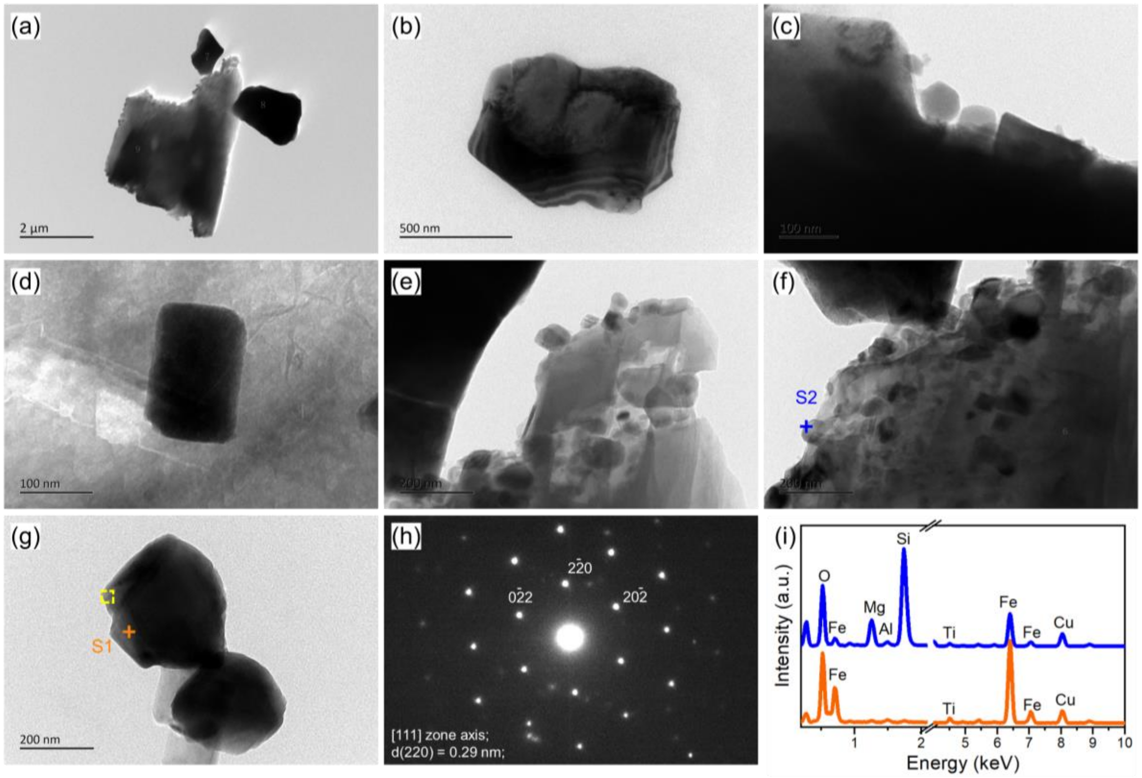

Figure S19. TEM images of magnetic minerals extracted from the sediment sample S4-1. (a)-(g) TEM images. (h) SAED pattern recorded from the [111] zone axis of the particle (indicated by yellow dashed box in (g)). (i) TEM-based EDXS spectra for individual particles (indicated by colored crosses and names in (f) and (g).

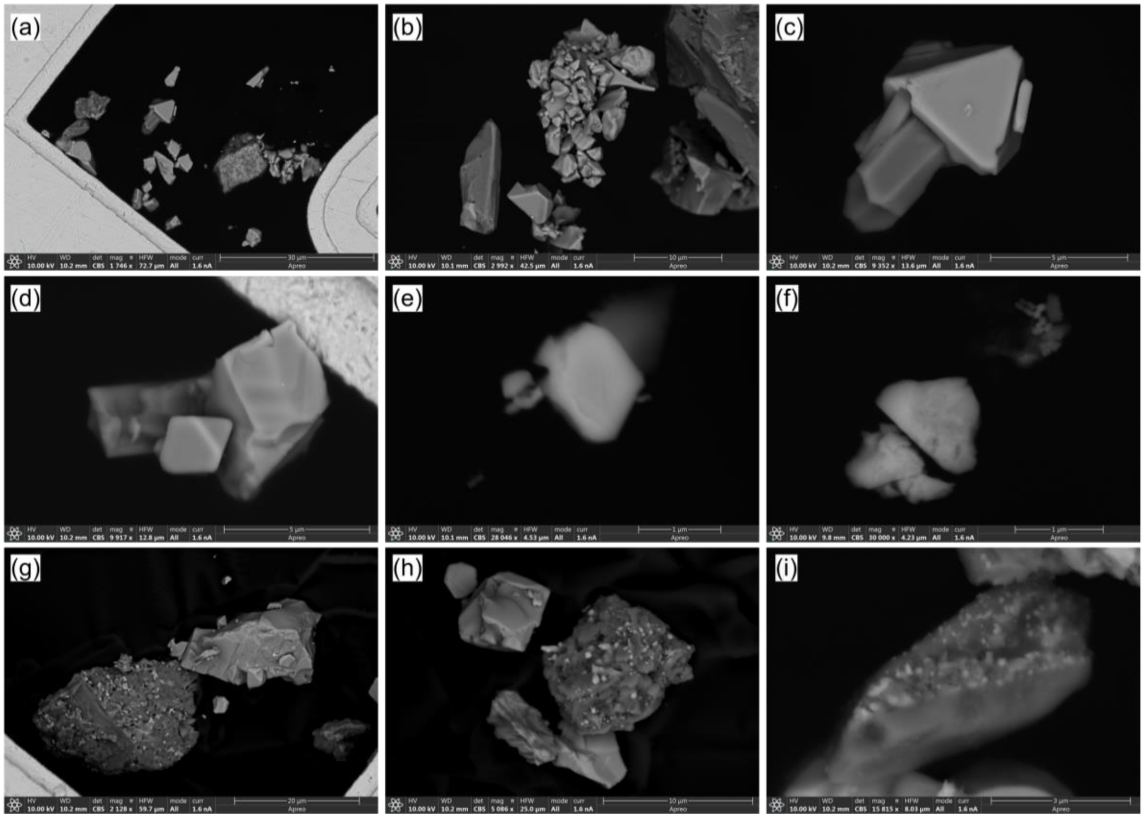

Figure S20. Backscattered SEM images of magnetic minerals extracted from the sediment sample S4-2.

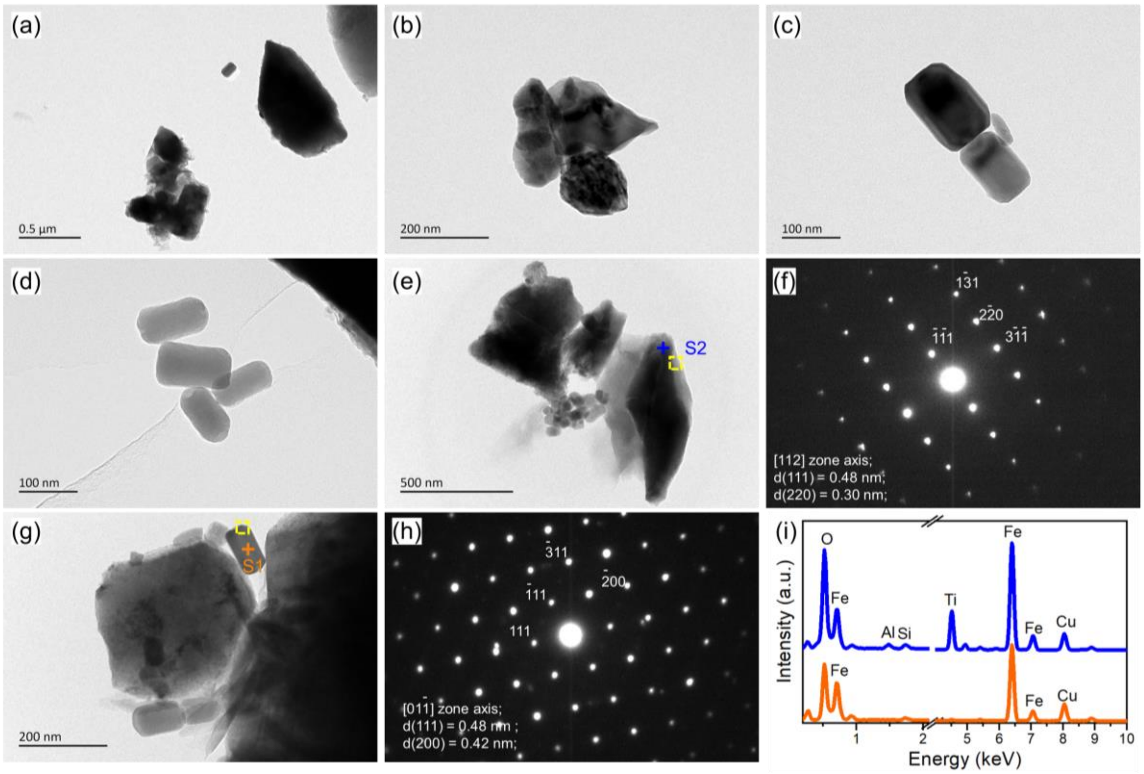

Figure S21. TEM images of magnetic minerals extracted from the sediment sample S4-2. (a)-(g) TEM images. (f) SAED pattern recorded from the [112] zone axis of the particle (indicated by yellow dashed box in (e)). (h) SAED pattern recorded from the [01$\bar{1}$] zone axis of the particle (indicated by yellow dashed box in (g)). (i) TEM-based EDXS spectra for individual particles (indicated by colored crosses and names in (e) and (g).

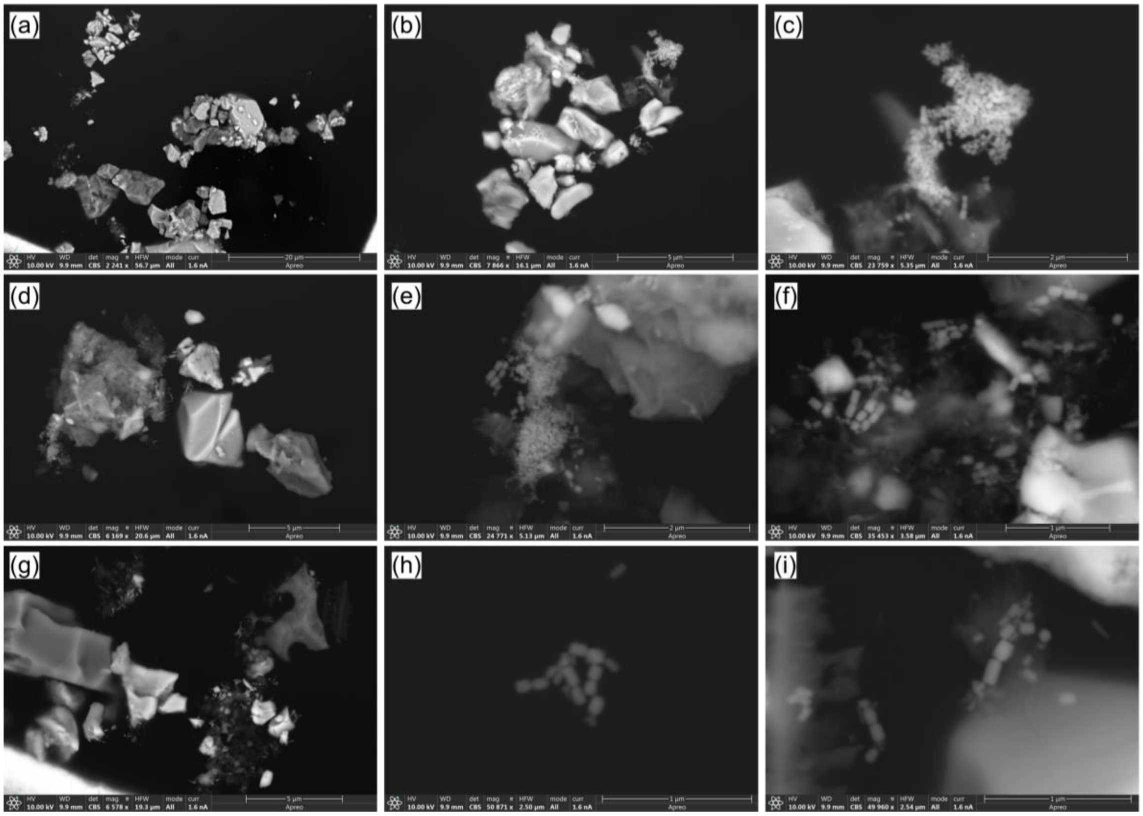

Figure S22. Backscattered SEM images of magnetic minerals extracted from the sediment sample S5-1.

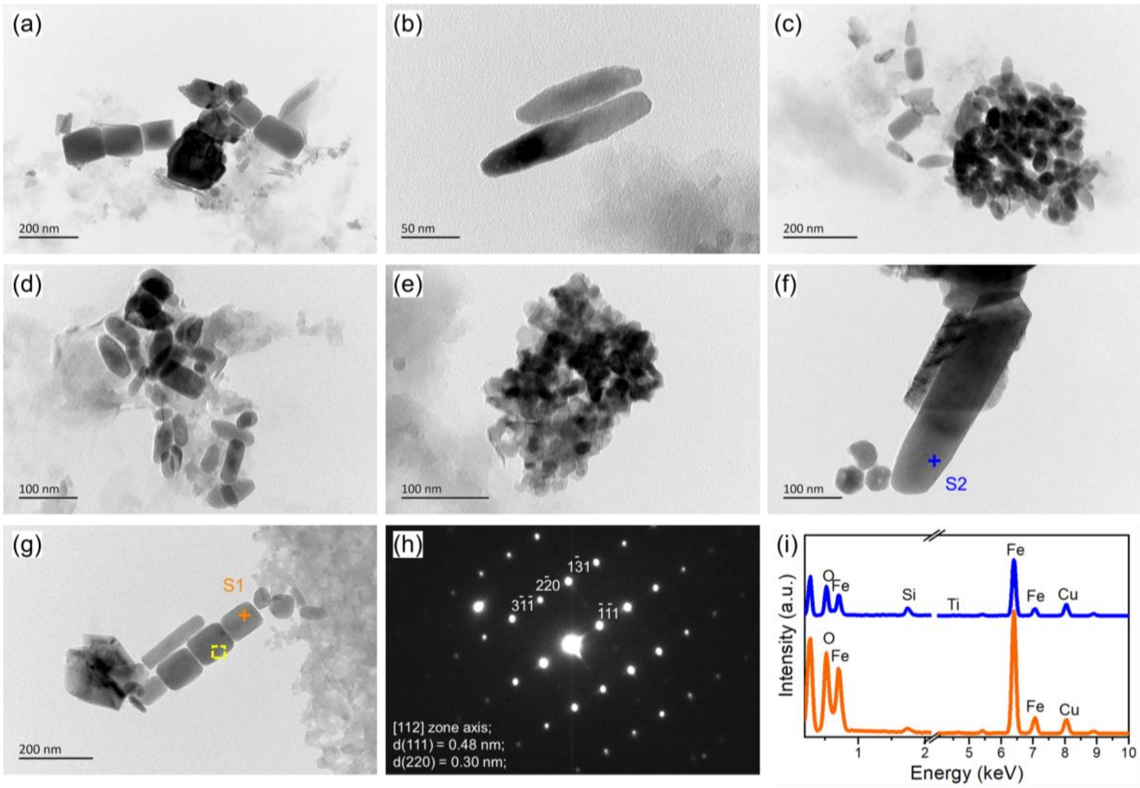

Figure S23. TEM images of magnetic minerals extracted from the sediment sample S5-1. (a)-(g) TEM images. (h) SAED pattern recorded from the [112] zone axis of the particle (indicated by yellow dashed box in (g)). (i) TEM-based EDXS spectra for individual particles (indicated by colored crosses and names in (f) and (g).

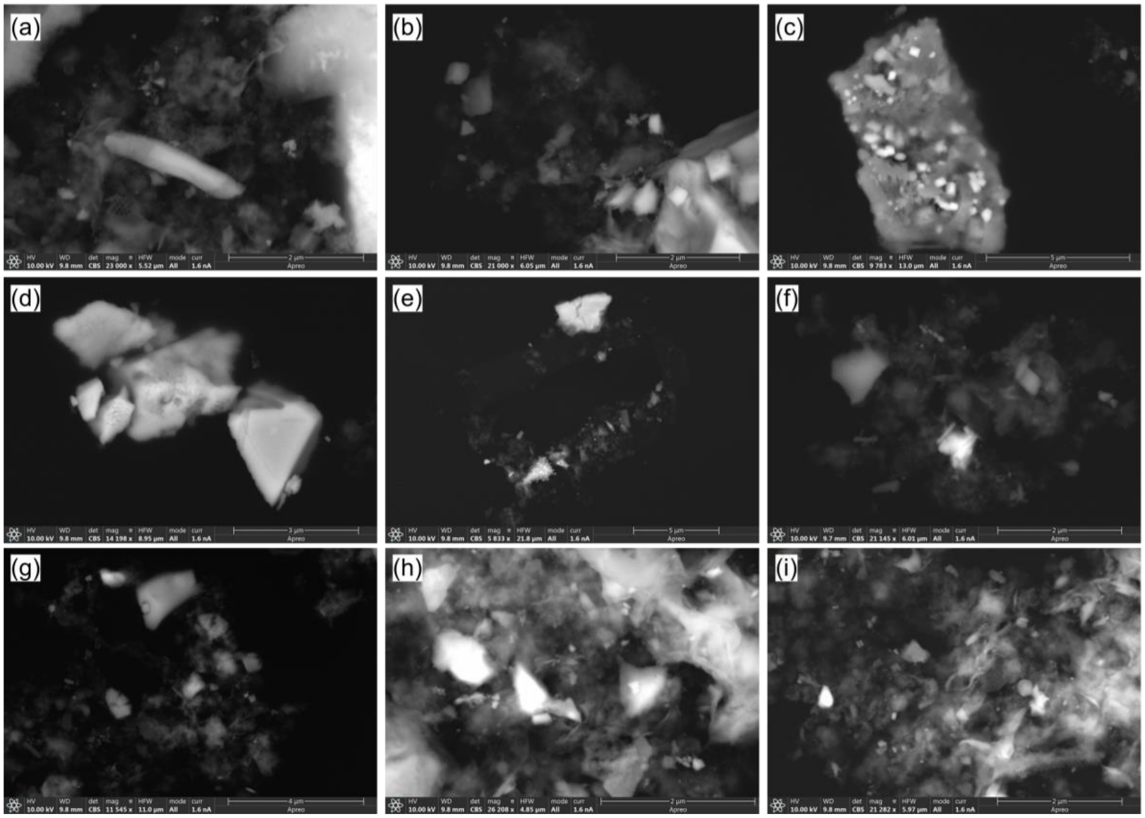

Figure S24. Backscattered SEM images of magnetic minerals extracted from the sediment sample S5-3.

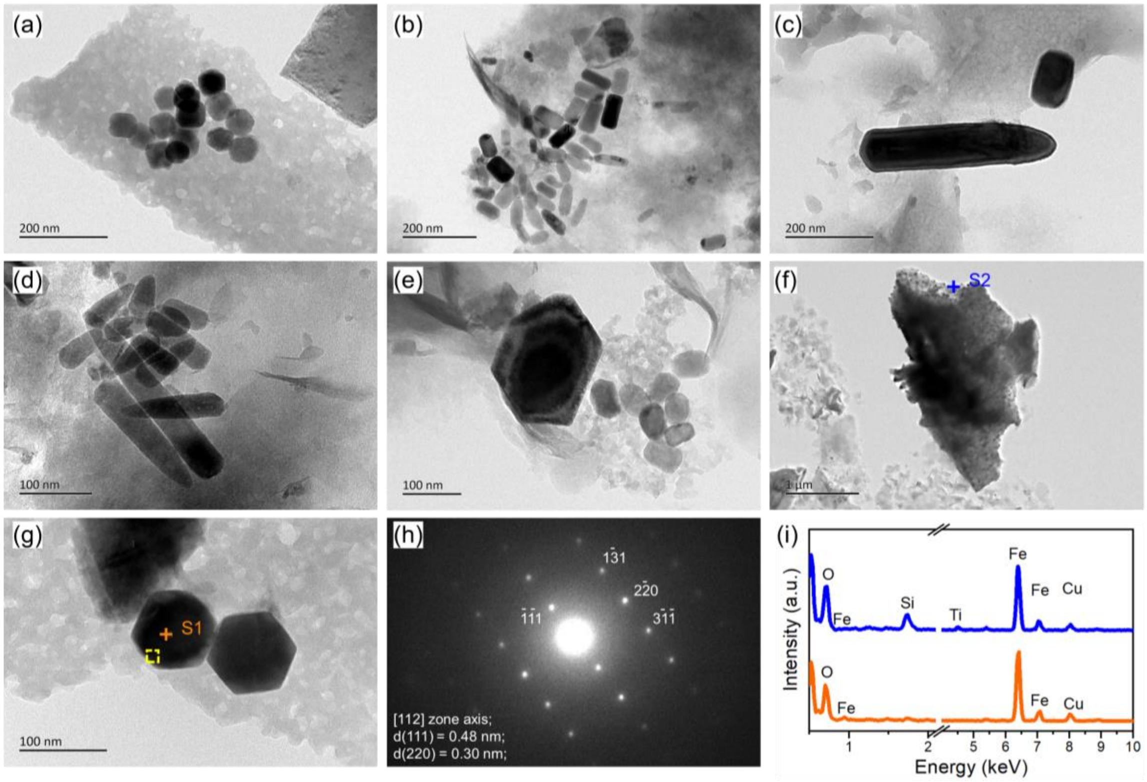

Figure S25. TEM images of magnetic minerals extracted from the sediment sample S5-3. (a)-(g) TEM images. (h) SAED pattern recorded from the [112] zone axis of the particle (indicated by yellow dashed box in (g)). (i) TEM-based EDXS spectra for individual particles (indicated by colored crosses and names in (f) and (g).

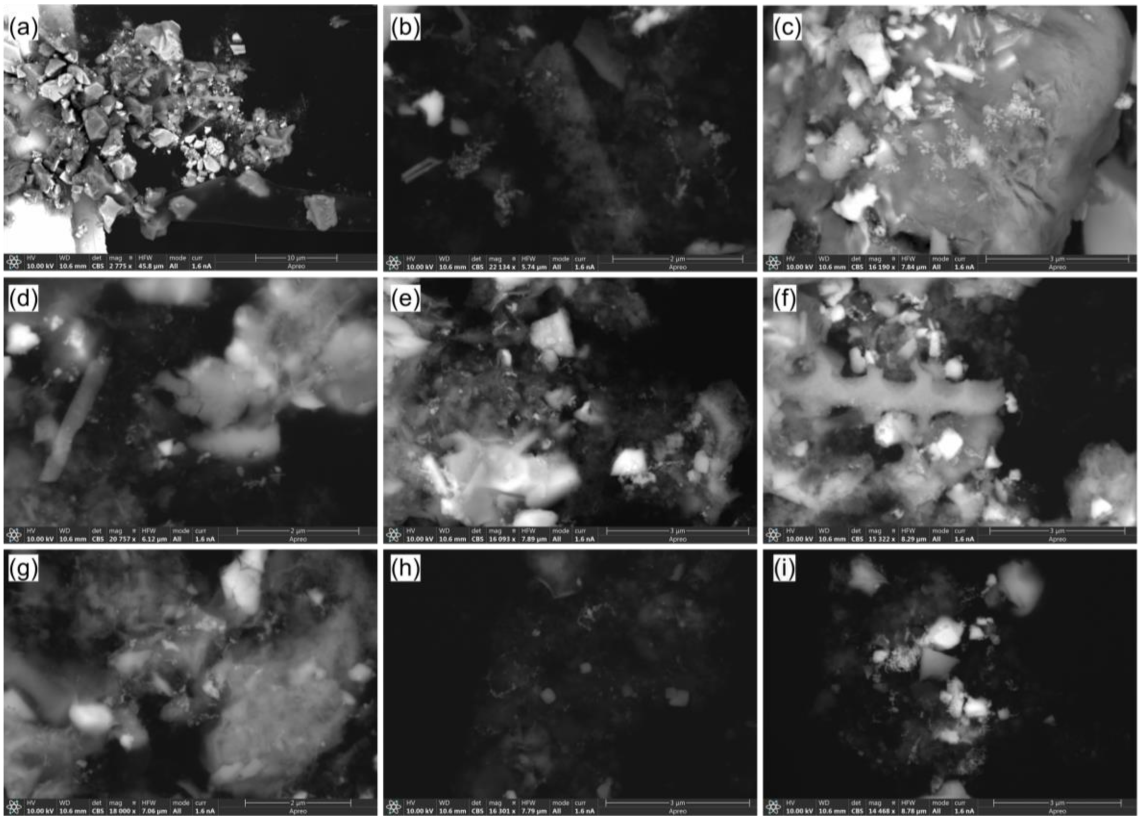

Figure S26. Backscattered SEM images of magnetic minerals extracted from the sediment sample S5-5.

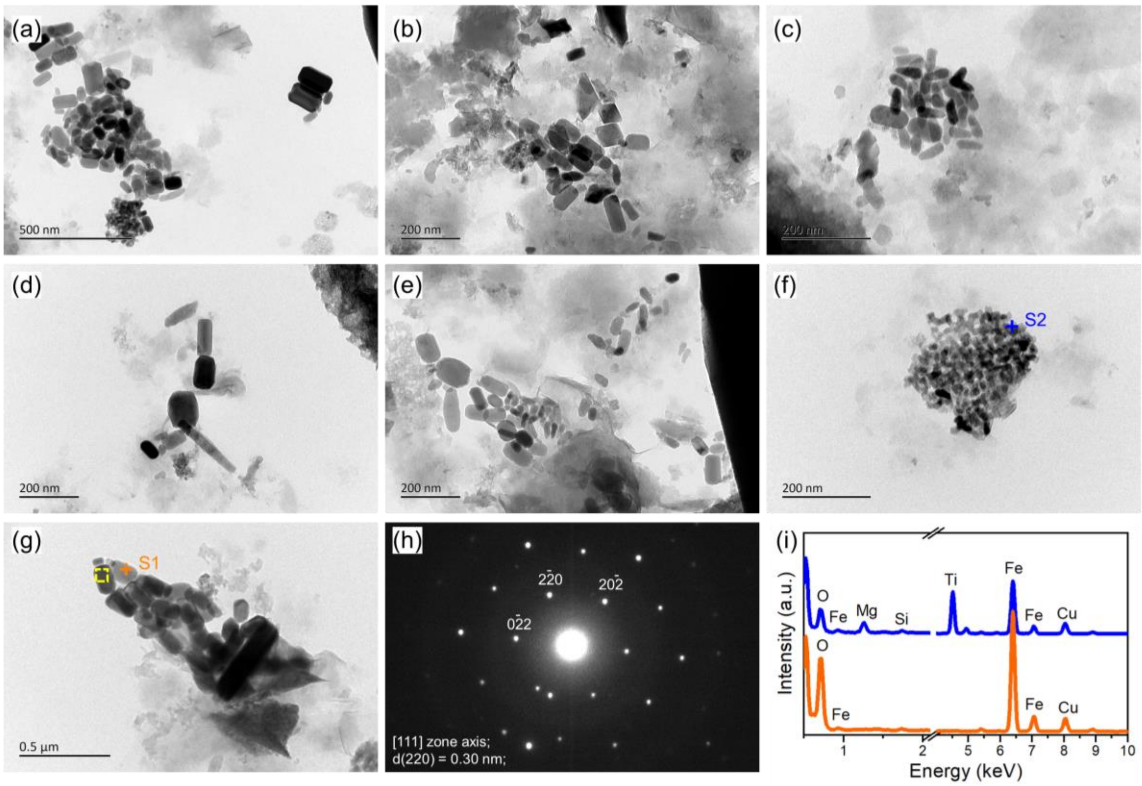

Figure S27. TEM images of magnetic minerals extracted from the sediment sample S5-5. (a)-(g) TEM images. (h) SAED pattern recorded from the [111] zone axis of the particle (indicated by yellow dashed box in (g)). (i) TEM-based EDXS spectra for individual particles (indicated by colored crosses and names in (f) and (g).

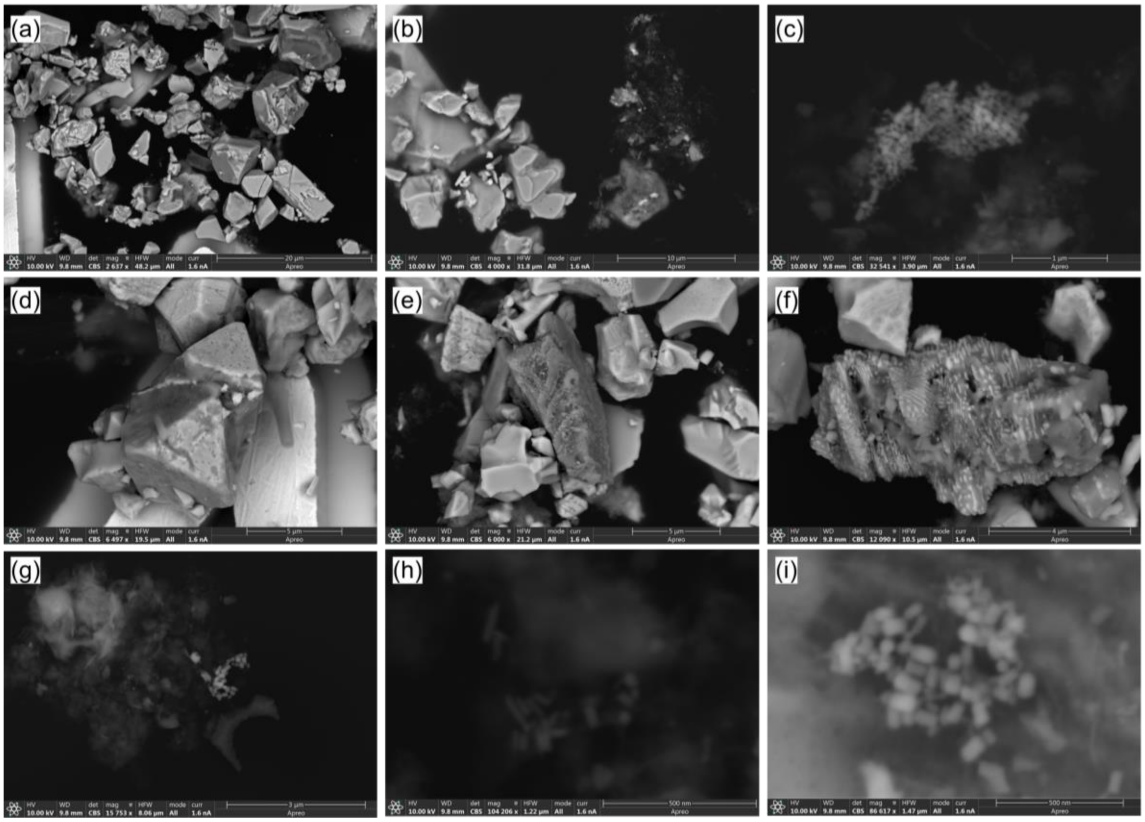

Figure S28. Backscattered SEM images of magnetic minerals extracted from the sediment sample S5-9.

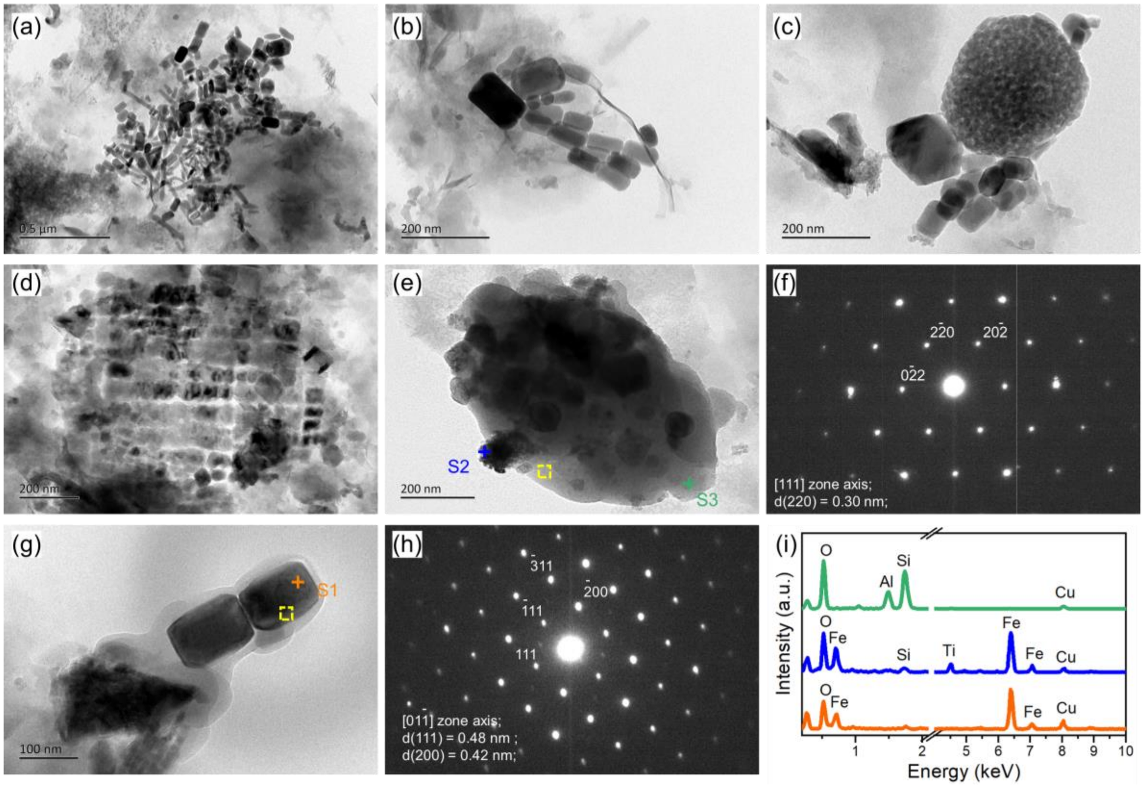

Figure S29. TEM images of magnetic minerals extracted from the sediment sample S5-9. (a)-(e), (g) TEM images. (f) SAED pattern recorded from the [111] zone axis of the particle (indicated by yellow dashed box in (e)). (h) SAED pattern recorded from the [01̄1] zone axis of the particle (indicated by yellow dashed box in (g)). (i) TEM-based EDXS spectra for individual particles (indicated by colored crosses and names in (e) and (g).

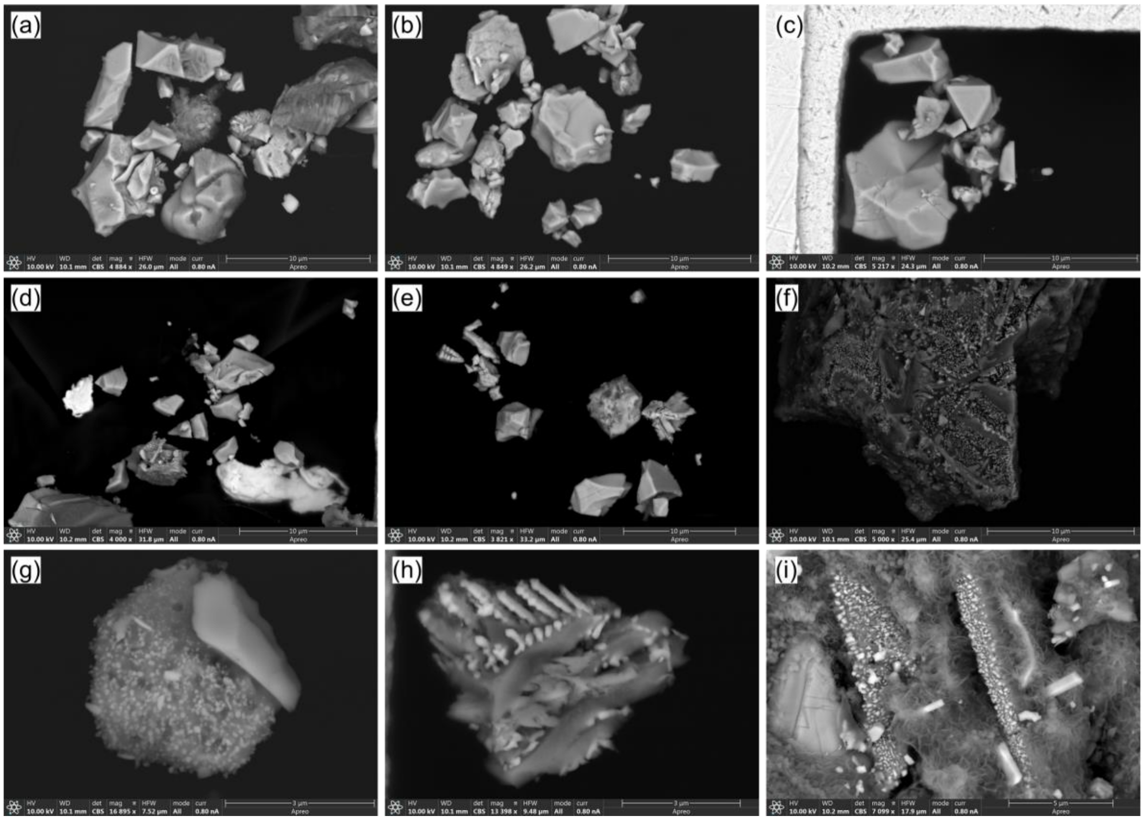

Figure S30. Backscattered SEM images of magnetic minerals extracted from the sediment sample S6-2.

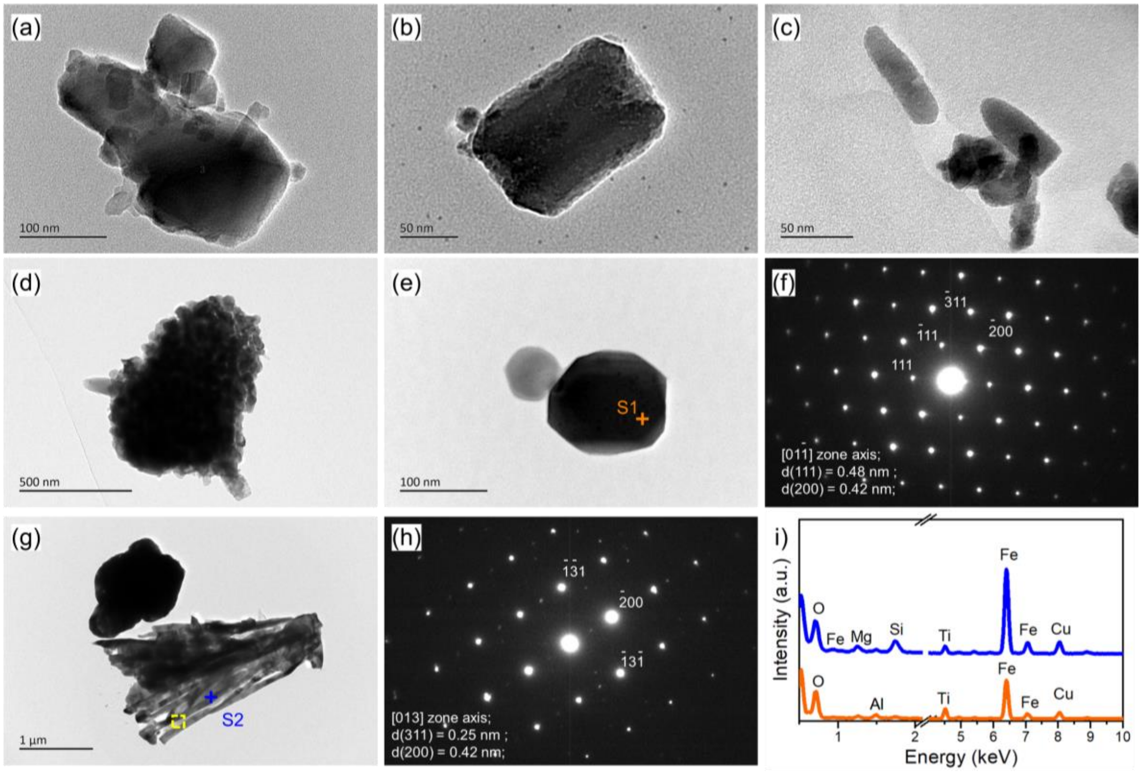

Figure S31. TEM images of magnetic minerals extracted from the sediment sample S6-2. (a)-(e), (g) TEM images. (f) SAED pattern recorded from the [01̄1] zone axis of the particle (indicated by yellow dashed box in (e)). (h) SAED pattern recorded from the [013] zone axis of the particle (indicated by yellow dashed box in (g)). (i) TEM-based EDXS spectra for individual particles (indicated by colored crosses and names in (e) and (g).

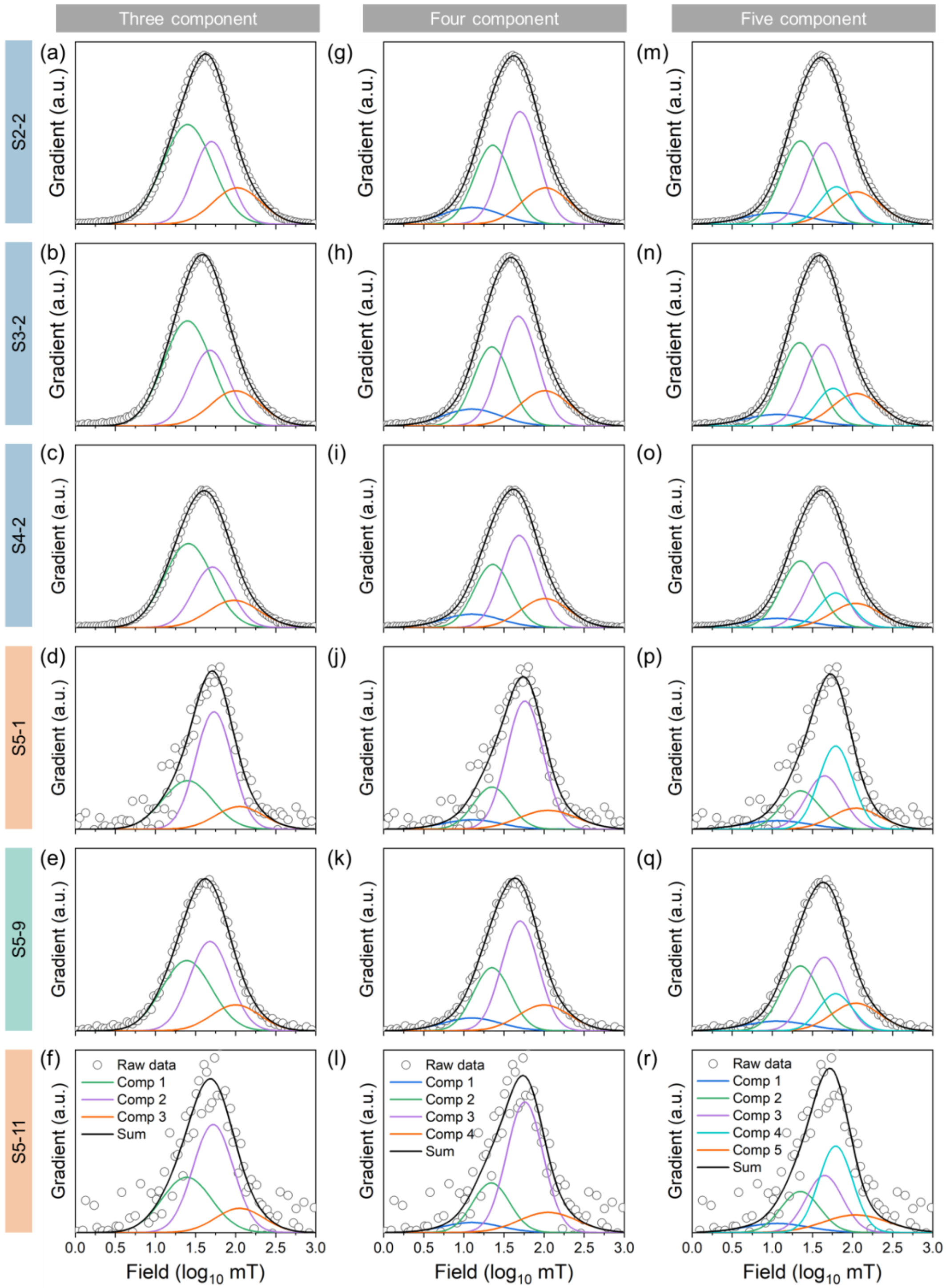

Figure S32. Gradient of IRM-Unmixing component acquisition plot for six representative samples with three strategies selected from glacial periods MIS 2 (S2-2, (a), (g), and (m)), MIS 3 (S3-2, (b), (h), and (n)), MIS 4 (S4-2, (c), (i), and (o)), relative warm MIS 5a (S3-2, (d), (j), and (p)) and MIS 5e (S3-2, (e), (k), and (q)), and cold MIS 5d (S3-2, (f), (l), and (r)). The first, second, and third columns are gradient of IRM-unmixing component acquisition plot with three, four and five magnetic coercivity components, respectively.

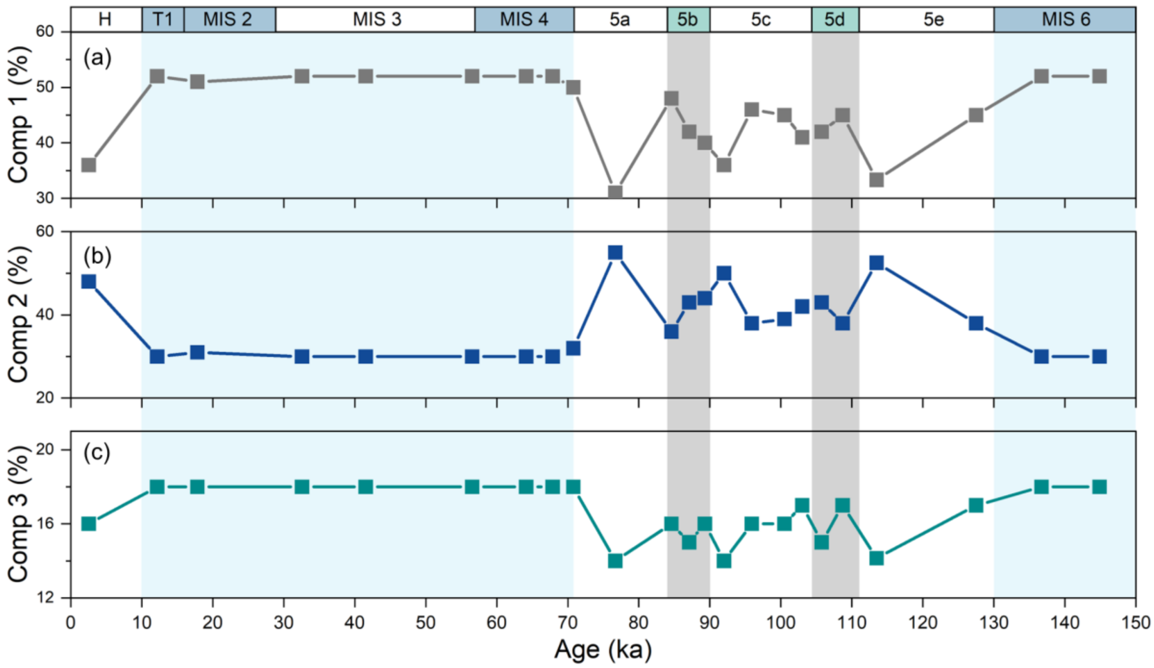

Figure S33. Temporal variations of proportion for three magnetic components unmixed from IRM acquisition curves for core MD11-3353 over the past 150 kyrs. Comp 1 has the lowest coercivity ($B_{1/2}$ = ~24.90 mT) and a DP value of ~0.31 that represent coarse detrital vortex state titanomagnetites. Comp 2 ($B_{1/2}$ = ~50.06 mT, DP = ~0.24) corresponds to a mixture of silicate-hosted SD titanomagnetite particles and magnetofossils. Comp 3 has the highest coercivity with a $B_{1/2}$ value of ~105.45 mT and a DP value of ~0.31, which might correspond to terrigenous maghemite, maybe mixed with a few high-coercivity magnetic minerals (e.g., hematite) which were not detected by electron microscopic observations or lost during the magnetic extraction, or both. Light blue and grey shadings outline the glacial periods (i.e., MIS 6, MIS 4-2, and T1) and cold substages during MIS 5 (i.e., MIS 5d and 5b), respectively.

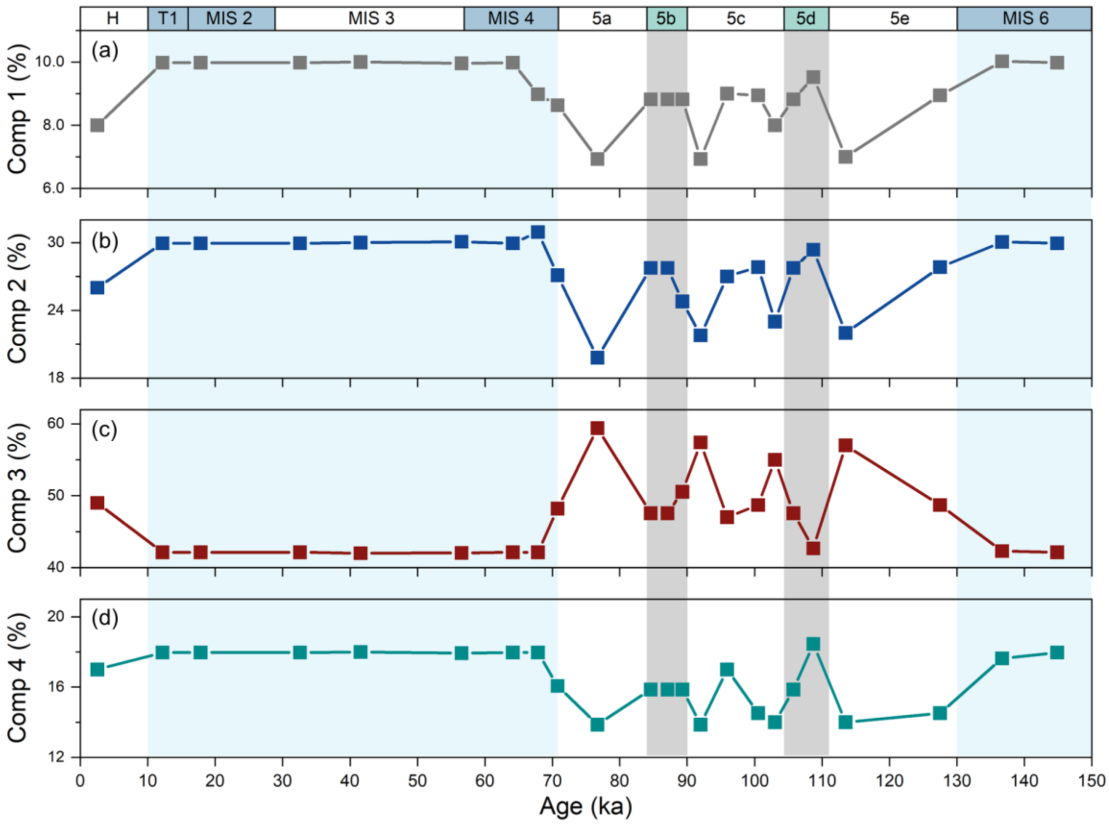

Figure S34. Temporal variations of four magnetic components unmixed from IRM acquisition curves for core MD11-3353 over the past 150 kyrs. Comp 1 has the lowest coercivity ($B_{1/2}$ = ~12.59 mT) and a DP value of ~0.36 that represent coarse detrital titanomagnetites. Comp 2 ($B_{1/2}$ = ~22.30 mT, DP = ~0.23) was interpreted as vortex state titanomagnetite. Comp 3 ($B_{1/2}$ = ~50.97 mT, DP = ~0.23) corresponds to a mixture of silicate-hosted SD titanomagnetite particles and magnetofossils. Comp 4 has the highest coercivity with a $B_{1/2}$ value of ~104.4 mT and a DP value of ~0.34, which might correspond to terrigenous maghemite, maybe mixed with a few high-coercivity magnetic minerals (e.g., hematite) which were not detected by electron microscopic observations or lost during the magnetic extraction, or both. Light blue and grey shadings outline the glacial periods (i.e., MIS 6, MIS 4-2, and T1) and cold substages during MIS 5 (i.e., MIS 5d and 5b), respectively.

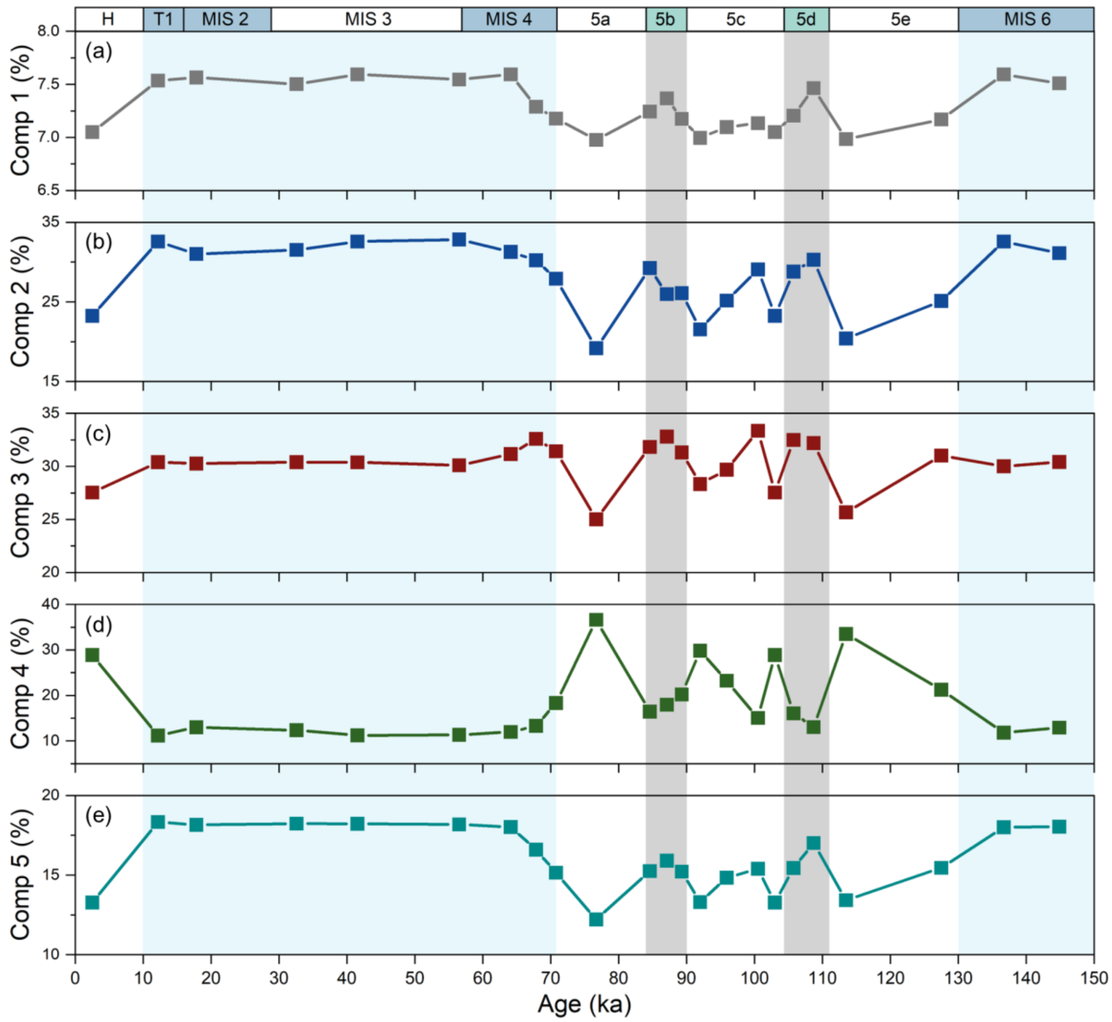

Figure S35. Temporal variations of proportion for five magnetic components unmixed from IRM acquisition curves for core MD11-3353 over the past 150 kyrs. Comp 1 with the lowest coercivities ($B_{1/2}$ = ~11.5 mT) and a DP value of ~0.40 represents the coarse detrital titanomagnetites. Comp 2 ($B_{1/2}$ = ~22.0 mT, DP = ~0.24) was interpret as vortex state titanomagnetites. Comp 3 ($B_{1/2}$ = ~43.4 mT, DP = ~0.22) correspond to a mixture of silicate-hosted SD titanomagnetite particles with low Ti contents and magnetofossils with equant (octahedral, 0.75 < width/length <1) crystals is ~40 mT. Comp 4 ($B_{1/2}$ = ~ 64.7 mT, DP = ~ 0.21) correspond to a mixture of SD titanomagnetite particles with high Ti contents and magnetofossils with elongated (hexagonal prism and bullet, width/length <0.75) crystals. Comp 5 has the highest coercivities with a $B_{1/2}$ value of ~104.4 mT and a DP value of ~0.34, which might correspond to terrigenous maghemite, maybe mixed with a few high-coercivity magnetic minerals (e.g., hematite) which were not detected by electron microscopic observations or lost during the magnetic extraction, or both. Light blue and grey shadings outline the glacial periods (i.e., MIS 6, MIS 4-2, and T1) and cold substages during MIS 5 (i.e., MIS 5d and 5b), respectively.

Table S1. Magnetic parameters of the twenty-three selected sediment samples from the core MD11-3353.

Sample	Age (ka)	B_c (mT)	B_{cr} (mT)	M_{rs}/M_s	B_{cr}/B_c	S-ratio	δ_{FC}	δ_{ZFC}	δ_{FC}/δ_{ZFC}	R_{sf}
S1-1	2.52	15.44	37.16	0.2598	2.4067	0.9471	0.2489	0.2440	1.0203	0.4571
S2-1	12.18	12.68	29.75	0.2144	2.3462	0.9795	0.2559	0.2588	0.9891	0.4470
S2-2	17.83	13.38	31.12	0.2197	2.3259	0.9816	0.2338	0.2337	1.0003	0.4487
S3-1	32.59	13.01	30.56	0.2159	2.3490	0.9808	0.2477	0.2467	1.0042	0.4457
S3-2	41.55	12.57	29.72	0.2123	2.3644	0.9816	0.2560	0.2598	0.9853	0.4515
S3-3	56.54	12.56	29.57	0.2146	2.3543	0.9795	0.2609	0.2648	0.9854	0.4515
S4-1	64.13	12.92	30.55	0.2149	2.3646	0.9828	0.2433	0.2436	0.9985	0.4461
S4-2	67.86	13.12	30.78	0.2221	2.3460	0.9807	0.2412	0.2397	1.0063	0.4430
S4-3	70.78	14.47	32.98	0.2403	2.2792	0.9747	0.2292	0.2282	1.0047	0.4529
S5-1	76.69	19.65	41.50	0.2989	2.1120	0.9850	0.2108	0.2002	1.0527	0.4626
S5-2	84.60	13.73	31.92	0.2363	2.3248	0.9771	0.2338	0.2310	1.0121	0.4545
S5-3	87.10	14.05	32.54	0.2306	2.3160	0.9780	0.2302	0.2251	1.0227	0.4512
S5-4	89.30	16.05	35.53	0.2663	2.2137	0.9720	0.2247	0.2235	1.0055	0.4633
S5-5	92.00	17.49	37.85	0.2710	2.1641	0.9746	0.2260	0.2170	1.0416	0.4568
S5-6	95.90	17.06	37.30	0.2911	2.1864	0.9699	0.2273	0.2219	1.0245	0.4672
S5-7	100.50	13.85	32.32	0.2287	2.3336	0.9770	0.2490	0.2433	1.0237	0.4516
S5-8	103.00	16.69	36.76	0.2753	2.2025	0.9782	0.2210	0.2131	1.0371	0.4545
S5-9	105.75	13.80	32.32	0.2243	2.3420	0.9810	0.2433	0.2421	1.0050	0.4522
S5-10	108.70	13.72	32.00	0.2231	2.3324	0.9743	0.2520	0.2530	0.9963	0.4537
S5-11	113.49	18.10	41.51	0.3058	2.2934	0.9876	0.2367	0.1958	1.0226	0.4659
S5-12	127.50	14.85	33.52	0.2462	2.2572	0.9790	0.2350	0.2330	1.0084	0.4554
S6-1	136.70	13.07	29.86	0.2156	2.2846	0.9818	0.2491	0.2543	0.9797	0.4536
S6-2	144.88	13.49	30.54	0.2181	2.2639	0.9817	0.2480	0.2490	0.9962	0.4513

Table S2. The relative content and abundance of detrital and biogenic magnetic minerals for the twenty-three selected sediment samples from the core MD11-3353.

Sample	Age (ka)	$SIRM_{1T}$ (Am^2/kg)	$(M_{rs}/M_{s})_{sample}$	$(M_{rs}/M_{s})_{detrital}$	$P_{biogenic}$	$SIRM_{1T\_biogenic}$ (10^{-3} Am^2/kg)	$P_{detrital}$	$SIRM_{1T\_detrital}$ (10^{-3} Am^2/kg)
S1-1	2.52	0.0037	0.2598	-	0.1965	0.7186	0.8035	2.9386
S2-1	12.18	0.0597	0.2144	0.2144	0	0	1	59.6560
S2-2	17.83	0.1110	0.2197	0.2197	0	0	1	111.0159
S3-1	32.59	0.0904	0.2159	0.2159	0	0	1	90.4303
S3-2	41.55	0.0599	0.2123	0.2123	0	0	1	59.8773
S3-3	56.54	0.0324	0.2146	0.2146	0	0	1	32.3692
S4-1	64.13	0.0738	0.2149	0.2149	0	0	1	73.8348
S4-2	67.86	0.0390	0.2221	-	0.0288	1.1233	0.9712	37.8946
S4-3	70.78	0.0214	0.2403	-	0.1097	2.3417	0.8903	19.0087
S5-1	76.69	0.0056	0.2989	-	0.3712	2.0880	0.6288	3.5376
S5-2	84.60	0.0198	0.2363	-	0.0918	1.8139	0.9082	17.9412
S5-3	87.10	0.0298	0.2306	-	0.0667	1.9845	0.9333	27.7854
S5-4	89.30	0.0135	0.2663	-	0.2257	3.0492	0.7743	10.4582
S5-5	92.00	0.0073	0.2710	-	0.2468	1.7961	0.7532	5.4817
S5-6	95.90	0.0056	0.2911	-	0.3363	1.8919	0.6637	3.7332
S5-7	100.50	0.0145	0.2287	-	0.0579	0.8371	0.9421	13.6173
S5-8	103.00	0.0147	0.2753	-	0.2658	3.9138	0.7342	10.8083
S5-9	105.75	0.0214	0.2243	-	0.0384	0.8221	0.9616	20.5888
S5-10	108.70	0.0254	0.2231	-	0.0331	0.8399	0.9669	24.5497
S5-11	113.49	0.0038	0.3058	-	0.4015	1.5404	0.5985	2.2958
S5-12	127.50	0.0132	0.2462	-	0.1360	1.7923	0.864	11.3874
S6-1	136.70	0.0611	0.2156	0.2156	0	0	1	61.0656
S6-2	144.88	0.1065	0.2181	0.2181	0	0	1	106.4874
Average		-	-	0.2157	-	-	-	-
Standard deviation		-	-	0.0023	-	-	-	-

Note: $(M_{rs}/M_{s})_{sample} = P_{biogenic}(M_{rs}/M_{s})_{biogenic} + P_{detrital}(M_{rs}/M_{s})_{detrital}$

where $(M_{rs}/M_{s})_{sample}$ represents the remanence ratio of one targeted sample, $P_{biogenic}$ is the percentage of biogenic magnetites (i.e., magnetofossils) in the sample, $P_{detrital}$ (e.i., 1- $P_{biogenic}$) is the percentage of detrital magnetic minerals in the sample, $(M_{rs}/M_{s})_{biogenic}$ is the remanence ratio related to magnetofossils, and $(M_{rs}/M_{s})_{detrital}$ is the remanence ratio related to detrital magnetic minerals. The $(M_{rs}/M_{s})_{detrital}$ value was calculated as the average of the value from eight glacial samples (S2-1, S2-2, S3-1, S3-2, S3-3, S4-1, S6-1, and S6-2), dominated by detrital titanomagnetites with nearly identical M_{rs}/M_{s} values. The $SIRM_{1T}$ resulting from the contribution of biogenic ($SIRM_{1T\_biogenic}$) and detrital ($SIRM_{1T\_detrital}$) magnetic minerals was calculated by $P_{biogenic}\times SIRM_{1T}$ and $P_{detrital}\times SIRM_{1T}$.